

Analytic relations assessing the impact of precursor knowledge and key mission parameters on direct imaging survey yield

PETER PLAVCHAN,¹ JOHN E. BERBERIAN JR.,^{1,2,3} STEPHEN R. KANE,⁴ RHONDA MORGAN,⁵ ELIAD PERETZ,⁶ AND SOPHIA ECONOMON^{7,8}

¹*Department of Physics & Astronomy, George Mason University, 4400 University Drive MS 3F3, Fairfax, VA 22030, USA*

²*Carter G. Woodson High School, 9525 Main St, Fairfax, VA 22031, USA*

³*University of Virginia, Charlottesville, VA, USA*

⁴*Department of Earth and Planetary Sciences, University of California, Riverside, CA 92521, USA*

⁵*Jet Propulsion Laboratory, California Institute of Technology, 4800 Oak Grove Dr, Pasadena, CA 91011, USA*

⁶*NASA Goddard Space Flight Center, Greenbelt, MD, USA*

⁷*Florida Institute of Technology, 150 W University Blvd, Melbourne, FL 32901*

⁸*Morton K. Blaustein Department of Earth and Planetary Sciences, John Hopkins University, 301 Olin Hall, 3400 N. Charles Street, Baltimore, MD 21218*

ABSTRACT

The Habitable Worlds Observatory will attempt to image Earth-sized planets in Habitable Zone orbits around nearby Sun-like stars. In this work we explore approximate analytic yield calculations for a future flagship direct imaging mission for a survey sample of uniformly distributed set of identical Sun-like stars. We consider the dependence of this exoplanet detection yield on factors such as η_{\oplus} , telescope diameter, total on-sky time, orbital phase and separation, inner working angle, flux contrast, desired signal-to-noise ratio, spectral resolution, and other factors. We consider the impact on yield and survey efficiency in the absence of and with precursor knowledge of the Earth-size analog exoplanets. In particular, for precursor knowledge we assume the exoplanet orbital phase at the time of observation can be optimized so as to only image the Earth-size analog exoplanet when it is outside the inner working angle. We find that the yield of flagship direct imaging missions such as Habitable Worlds Observatory will be inner-working angle limited for the estimated exoplanet yields, and will not be impacted by precursor knowledge given our assumptions presented herein. However, we find that the survey efficiency will be enhanced by precursor knowledge. We benchmark our analytic approximations against detailed simulations for coronagraphs and starshades carried out for the HabEx and LUVOIR missions concept studies, and find consistent conclusions. Our analytic relations thus provide quick estimates and derivatives of the impact of key mission parameter choices on exo-Earth yield when considering design trades that can supplement existing computational simulations.

Keywords: planetary systems – techniques: direct imaging

1. INTRODUCTION

Over the past three decades, more than 5500 exoplanets have been discovered to orbit other stars, and the pace of discovery is accelerating (Akeson et al. 2013). As time has progressed, the main methods for exoplanet detection have been continually refined and improved to increase sensitivity to smaller and less massive planets orbiting main sequence stars. The method of exoplanet direct imaging was first successful in imaging 2MASS 1207 b in Chauvin et al. (2004), with now over 60 exoplanets discovered via direct imag-

ing (Akeson et al. 2013), including the multiplanet system HR 8799 (Marois et al. 2008). Prior to the 2020 Astrophysics Decadal Survey, NASA undertook the study of four flagship mission concept studies led by four science and technology definition teams (STDTs), which produced reports submitted for consideration by the Decadal Survey (Gaudi et al. 2020; Team 2019; Meixner et al. 2019; Gaskin et al. 2019). Two of these mission concepts, HabEx and LUVOIR, considered the possibility of imaging other Earth-sized planets orbiting in the Habitable Zones (HZ) around nearby, Sun-like stars (hereafter exo-Earths) (Kasting et al. 1993; Kopparapu et al. 2013, 2014; Kane et al. 2016). The 2020 Astrophysics Decadal Survey has recommended the development program

for a future flagship direct imaging mission with a primary mirror of ~ 6 m (NAP 2023). NASA has in turn launched the GOMAP (Great Observatory MAturation Program) and the START (Science, Technology, Architecture Review Team) for the HWO (Habitable Worlds Observatory)¹.

Central to the scientific motivation for the Habitable Worlds Observatory, and predecessor mission concepts HabEx and LUVOIR, is the yield or number of exo-Earths these missions could be able to detect and characterize. As part of evaluating the feasibility of these mission concepts, detailed numerical simulations have been carried out to assess the yield of directly imaged exoplanets. In particular, a Standard Definitions and Evaluation Team was formed by NASA with joint members from the mission concepts to evaluate mission yields, including such definitions as a common standard for the assumed exoplanet demographics, the location of the Habitable Zone and exoplanet size categories (Morgan et al. 2019; Dulz et al. 2020; Kopparapu et al. 2018). One of the key quantities that drives these mission yields is the exo-Earth occurrence rate η_{\oplus} ; the smaller this value, the larger a telescope will be needed. Direct imaging mission studies place much focus on understanding the impact of η_{\oplus} and its corresponding uncertainty on the yield. Recent estimates of η_{\oplus} from the Kepler mission have declined but also increased in precision and knowledge (e.g., Bryson et al. 2021; Zink et al. 2019, and references therein), due to improvements of our understanding of the reliability and completeness of the Kepler mission exoplanet search, and also due to improvements in knowledge of our stellar parameters, particularly the stellar radius (Plavchan et al. 2014) with the release of Gaia DR2 and eDR3 (Gaia Collaboration et al. 2016; Bailer-Jones et al. 2018; Gaia Collaboration et al. 2018, 2021). Many other factors impact mission yield and design, including astrophysical considerations such as the actual distribution of nearby stars and spectral types and exoplanet system demographics, and also mission parameters such as requirements on spectral resolution and grasp, signal to noise ratio, overhead time, assumed flux contrast ratio, etc. as explored in detailed simulations in Stark et al. (2014, 2015) and Peretz et al. (2021). The HabEx and LUVOIR mission concepts also considered the possibility that precursor knowledge of the existence, or lack thereof, could impact mission yield, such as could be provided by radial velocities or astrometry. In particular for LUVOIR B and the three HabEx mission concepts, including those with a starshade, Morgan et al. (2021) carried out detailed simulations assessing this impact. They found that while precursor knowledge had a minor impact on mission yield, it did significantly impact survey efficiency. Assuming an intermediate

telescope diameter between HabEx and LUVOIR, Guimond & Cowan (2018) explored through simulations the impact of false-positives and precursor knowledge on a direct imaging survey yield of Earth-mass analogs. They expanded upon the work in Stark et al. (2014, 2015), considering the exoplanet yield of planets besides exo-Earths, and found that 77% of imaged exoplanets that would at first appear to be exo-Earth analogs at HZ projected orbital separations were in fact other planets in the system at different true orbital separations and planet radii. They found that precursor knowledge of the orbits would help substantially in reducing this false-positive rate and consequently improving the exoplanet yield.

Estimating the yield of a future flagship direct imaging mission is a well-trodden subject of inquiry as different mission concepts have been proposed over the preceding decades, dating back to at least Brown (2004a,b, 2005). For example, Agol (2007) explored detailed analytic estimates of direct imaging mission yield, employing a differential-based formalism of yield estimates, assuming a local stellar density and initial mass function (IMF), a lognormal planet size distribution, and investigating the optimization of yield as a function of observing wavelength, exo-zodiacal (zodi) levels, stellar metallicity, and other considerations, but did not explore the impact of precursor knowledge on survey yield or efficiency. They applied their analytic relations to a suite of mission concepts under consideration at the time. Next, Brown & Soummer (2010) explored the exo-Earth yield if the design reference mission for the James Webb Space Telescope (JWST) had been equipped with a starshade, employing a sequential observation approach to estimate the probability of observing an exo-Earth with each subsequent observation based upon the outcome of prior observations, deriving an estimate for survey completeness. Catanzarite & Shao (2011) expanded upon this work to investigate different observing strategies for detection and confirmation of exo-Earths with a star-shade equipped JWST. Lyon & Clampin (2012) employed an analysis investigating the yield for a set of different direct imaging mission aperture sizes for a specific set of the nearest stars, employing numerical yield estimates from a set of analytic scaling dependencies on various mission parameters. Next, Savransky (2013) developed a set of numerical simulation for estimating exoplanet yield for a direct imaging mission that could be customized for any mission concept with an end-to-end simulation framework, including applying exoplanet demographics from the *Kepler* mission, and specifically applied this to the Roman mission concept (formerly WFIRST and AFTA) for exoplanets in general, and not specifically exo-Earths. Finally, Kopparapu et al. (2018) used the SAG13 exoplanet demographics from *Kepler* to estimate direct imaging mission yields of different exoplanet types, although those demographics were super-ceded by the exoplanet population demograph-

¹ <https://science.nasa.gov/astrophysics/programs/gomap/>

ics in [Dulz et al. \(2020\)](#) and the final HabEx and LUVOIR yield estimates ([Gaudi et al. 2020](#); [Team 2019](#); [Morgan et al. 2019](#)).

Several studies have also looked at the impact on precursor knowledge on direct imaging exoplanet yield. We define precursor knowledge in this work to be knowledge both of which stars have planets of interest for direct imaging, and also sufficient knowledge of projected orbital separation to image the planets outside the inner working angle when targeted. [Traub et al. \(2016\)](#) explored the direct imaging yield for the Roman mission, where targets were all known prior to imaging, and taking into account specific coronagraphic mask architectures with lab-based sensitivity curves as a function of angular separation. [Shao et al. \(2010\)](#) explored the impact of precursor knowledge from astrometry for a former mission concept called the Occulting Ozone Observatory with a 1.1 m aperture, and in particular identified that the yield of exoplanets could be increased by a factor of 4-5 from precursor knowledge. However, [Savransky et al. \(2009\)](#) conducted numerical simulations of the exo-Earth yield for a future direct imaging mission (in this case the THEIA concept), and found that precursor knowledge from astrometry did not significantly impact mission yield, but did significantly improve direct imaging survey mission efficiency. They also explicitly assess the impact of yield from η_{\oplus} , finding that precursor knowledge provides increasing benefits for decreasing exo-Earth occurrence rates. [Davidson \(2011\)](#) assessed the impact of precursor knowledge from astrometry on the number of re-visits required (survey efficiency) for a set of seven direct imaging targets, finding that precursor knowledge decreases the required number of revisits for a coronagraphic mission and to a lesser extent for an external occulter for a set of four specific prior mission concepts.

In this work, we develop a toy model to derive analytic relations for estimating the exo-Earth yield of a direct imaging mission and its dependence on different mission parameters and specifically the impact of precursor knowledge, relying on a set of a few simplifying assumptions. Our intent is to provide a set of relations derived from our toy model to guide and help validate the more detailed simulations carried out previously for HabEx and LUVOIR, and to be further refined for the Habitable Worlds Observatory in the future. Our analytic treatment is simpler than in [Agol \(2007\)](#); however, we additionally explore analytic yield dependence on precursor knowledge, complementing the aforementioned works that looked at the impact of precursor knowledge through simulations or specific direct imaging mission architectures. We also specifically look at the parameters for which a direct imaging survey will be in a “photon noise limited” or an “inner working angle limited” regime, and the transition between the two.

First, we assume circular orbits, which are common for compact terrestrial planetary systems as found by the Kepler mission as inferred from their mutual inclination and transit duration distributions [Lissauer et al. \(2011\)](#); [Shabram et al. \(2016\)](#); [Fang & Margot \(2012\)](#); [Plavchan et al. \(2014\)](#), but larger Jovian planets can more commonly exhibit more eccentric orbits. [Kane \(2013\)](#) in particular explored the impact eccentricity had on whether or not a planet falls outside the inner working angle of a direct imaging survey. Second, we also assume all stars are single Sun-like stars with identical location HZ orbits with exo-Earths located at 1 au. In other words, we do not marginalize over distributions in planet radius, insolation flux / orbital distance, nor stellar spectral type. [Crepp & Johnson \(2011\)](#) explored the impact of exoplanet direct imaging yield as a function of stellar spectral type, but primarily for ground-based direct imaging instrumentation. Third, when we consider the impact of precursor knowledge on mission yield, we assume perfect and complete knowledge – e.g. we do not consider a scenario in which only a fraction of target stars have precursor knowledge, nor when the orbital knowledge is insufficient to fully predict if an exoplanet is outside an inner working angle, such as can be the case with the radial velocity method with an unknown orbital inclination. We also do not consider the impact of planet multiplicity on exoplanet yield, where planets at larger orbital separations can mistakenly appear to be projected into Habitable Zone orbits in a single visit ([Guimond & Cowan 2018](#)).

Next, we adopt a simplified noise model where the contributions from exo-zodis and speckles (host starlight suppression residuals) scales with the photon noise, and derive a scaling factor by fitting our model to exposure time estimates made with EXOSIMS ([Morgan et al. 2019](#)). Our model reproduces the EXOSIMS exposure times to within 20% (see §2.1 and §7.1). While this model effectively ignores Solar System zodiacal light noise contributions, more detailed computational simulations show >50% disagreement amongst themselves for the same target and instrument configuration ([Morgan et al. 2019](#)), and is thus an adequate model for the purposes of developing our simplified analytic approach. Finally, we do not model the impact of obscured vs. un-obscured apertures, and segmented vs. single-aperture telescope designs, which has been shown to also introduce important changes in yield as a function of telescope diameter ([NAP 2023](#)).

In §2, we derive a basic yield model for direct imaging surveys, one that is only limited by photon noise (e.g. a negligible inner working angle), without and with precursor knowledge in turn. In §3, we enhance that “photon-noise limited” model by evaluating the impact of the telescope inner working angle on the random observations of an uninformed survey – e.g. assessing the fraction of survey time that is

lost when a target for which we do not know whether or not the orbital ephemerides lies inside the inner working angle. In §4, we derive equations to describe the lower bound on the telescope diameter specified by the required yield and the inner working angle, in the “inner working angle limited” regime. In §5, we investigate the transition between the “photon noise limited” and “inner working angle limited” regimes to assess under what direct imaging survey parameters a given survey would be photon noise or inner working angle limited. In §6, we summarize our key results to be useful in evaluating future mission architecture design trades. In §7, we compare these analytic relations to more detailed numerical simulations carried out in prior work. In §8 we present our conclusions.

2. BASIC PHOTON NOISE YIELD MODEL

In this section, we establish a basic exo-Earth yield model without precursor knowledge and without an inner working angle requirement, and accounting only for sufficient detected photons from the targeted planets. In other words, we first assume the planet is always imaged outside the inner working angle, and after we construct this model, we then consider the impacts of precursor knowledge in §2.2, and the impact of inner working angle in §3.

2.1. No Precursor Knowledge

First, we consider the case of no precursor knowledge: a scenario in which we have no information about the distribution of exo-Earths, and thus target stars are searched at random. We first define as expected: $N_{\oplus} = N_* \eta_{\oplus}$, where N_* is the number of stars we are surveying, and N_{\oplus} is the number of those stars that host exo-Earth planets. As stated in §1 for simplification in our analytic model, we assume all exo-Earths are located at an orbital distance equal to 1 au from their host stars, and all host stars are identical and Sun-like, e.g. $1M_{\odot}$ and $1R_{\odot}$. Further, we assume any information about the insolation flux, size range, or other properties of the exo-Earths are incorporated into the value of η_{\oplus} . In other words, we do not consider a range of insolation flux / habitable zone orbital distance, planet size, or host star spectral type distributions, as explored in Kane (2013); Crepp & Johnson (2011).

Assuming a uniform random distribution of N_* identical stars, we express the stellar density as

$$\rho_* = \frac{N_*}{\frac{4}{3}\pi D_{\text{lim}}^3}, \quad (1)$$

where D_{lim} is the limiting distance of our hypothetical survey (due to the assumption of identical stars, . We can also express this in terms of the density of exo-Earths as $\rho_{\oplus} = \rho_* \eta_{\oplus}$, so

$$\rho_{\oplus} = \rho_* \eta_{\oplus} = \frac{N_{\oplus}}{\frac{4}{3}\pi D_{\text{lim}}^3} \quad (2)$$

Second, we can next define that the total on-sky time $T = \sum_{k=1}^{N_*} t_k$, where t_k is the time spent on the k th star and T is the constant survey duration, and where we assume that survey duration is constant, ignoring mission extensions and assuming the mission surveys all N_* stars. Third, we define $R(\nu)$ to be the bolometric rate at which a star isotropically radiates light over the wavelength range of interest, in photons per second, for some central frequency ν . We also assume a constant star-planet flux contrast ratio K , e.g. identical Earth-size planets orbiting our assumed and simplistic local universe of identical stars. Then, the rate R_e , in photons/sec, at which our survey telescope detects reflected light from the k th planet would be

$$R_e = RK \frac{\pi(d/2)^2 \varepsilon}{4\pi D_k^2} = \frac{RKd^2 \varepsilon}{16D_k^2} \quad (3)$$

where D_k is the distance in meters from earth to the k th star and its planet, where d is the diameter in meters of the telescope, and where $\varepsilon(f)$ is the telescope efficiency as a function of frequency, including filters, atmospheric interference, etc., and assumed to have negligible throughput degradation over the course of the survey duration.

Next, most direct imaging missions have some $SNR \geq SNR_0$ requirement in the continuum flux for each planet observed. We assume the bounding scenario where observations achieve the minimum $SNR = SNR_0$ requirement. Reaching that SNR for the k th star requires an exposure time

$$t_k \approx SNR_0^2 \frac{R_e + 2B_k}{R_e^2}$$

where B_k is the count rate for all sources of background. This is a restatement of the CCD SNR equation solved for the exposure time, with the assumption of zero noise detectors, and combining any scattered light, zodiacal, exo-zodiacal and similar background noise into a single term B_k . We next make a simplifying assumption that B_k scales linearly with R_e and thus also the stellar flux R , such that B_k can be expressed as $B_k = \frac{1}{2}r'R_e$ and where r' can be tuned for a different set of assumed noise levels. This is equivalent to assuming there is no systematic noise floor from Solar System zodiacal light or otherwise, and that independent of the stellar brightness, there is a constant exo-zodiacal contribution for every star that can be combined with the scattered light contribution to the background noise that will scale with the stellar brightness, and that the achieved flux contrast for the direct imaging mission instrument contributes a constant noise term to the planet flux measurement. Further, we ignore for simplicity how this flux contrast varies with angular separation, and assume for example that a ‘dark hole’ (Give’on et al. 2007) of constant flux contrast K can be created at any location outside an inner working angle for the assumed constant

background noise term. Then, we have:

$$t_k = \text{SNR}_0^2 \frac{1+r'}{R_e}.$$

To simplify the expression, let $r \equiv 1+r'$ and thus $B_k = \frac{1}{2}(r-1)R_e$. Then:

$$t_k = \frac{r\text{SNR}_0^2}{R_e} = \frac{16r\text{SNR}_0^2 D_k^2}{RKd^2 \varepsilon}. \quad (4)$$

We discuss the validity of adopting this noise model further in §7.1. Because the stars are randomly distributed throughout a sphere of radius D_{lim} , we can divide the sphere up into N_* spherical shells of equal volume, and assume that there is exactly one star contained in each spherical shell (e.g. we are ignoring any stellar binarity). Each shell would have volume $\frac{4\pi}{3N_*} D_{\text{lim}}^3$. Therefore, the outer radius of the k th spherical shell D_k must satisfy

$$\begin{aligned} \frac{4\pi}{3} D_k^3 &= \frac{4k\pi}{3N_*} D_{\text{lim}}^3 \\ D_k^3 &= \frac{k}{N_*} D_{\text{lim}}^3 = \frac{3k}{4\pi\rho_* D_{\text{lim}}^3} D_{\text{lim}}^3 = \frac{3k}{4\pi\rho_*} \\ t_k &= \frac{16r\text{SNR}_0^2 D_k^2}{RKd^2 \varepsilon} = \frac{16r\text{SNR}_0^2}{RKd^2 \varepsilon} \left(\frac{3k}{4\pi\rho_*} \right)^{2/3} \end{aligned} \quad (5)$$

We assume the planet to be located at the outer border of the spherical shell; this is a worst-case scenario for an observer. Because the total on-sky time for a survey must be equal to the sum of the integration times (ignoring slew time, overheads, etc.),

$$T = \frac{16r\text{SNR}_0^2}{RKd^2 \varepsilon} \left(\frac{3}{4\pi\rho_*} \right)^{2/3} \sum_{k=1}^{N_*} k^{2/3} \quad (6)$$

So, because T is fixed, we know that

$$d^2 = \frac{16r\text{SNR}_0^2}{RKT \varepsilon} \left(\frac{3}{4\pi\rho_*} \right)^{2/3} \sum_{k=1}^{N_*} k^{2/3} \quad (7)$$

2.1.1. With simple approximation

We approximate

$$\sum_{k=1}^{N_*} k^{2/3} \approx \int_0^{N_*} x^{2/3} dx = \frac{3}{5} N_*^{5/3} \quad (8)$$

Because the first is effectively a Riemann sum of the second, this is a reasonable approximation. However, it will have a very high percent error for low values of N_* . Therefore, we assume that N_* is large, greater than 100. (A value of $N_* = 100$ yields a 0.83% error, and percent error improves

with increasing N_* .)

So,

$$d^2 = \frac{16r\text{SNR}_0^2}{RKT \varepsilon} \left(\frac{3}{4\pi\rho_*} \right)^{2/3} \frac{3}{5} N_*^{5/3} \quad (9)$$

$$\begin{aligned} d &= 4\text{SNR}_0 \left(\frac{3}{4\pi\rho_*} \right)^{1/3} \sqrt{\frac{3rN_*^{5/3}}{5RKT \varepsilon} \eta_{\oplus}^{-5/3}} \\ d &= 4\text{SNR}_0 \eta_{\oplus}^{-5/6} \sqrt[6]{\frac{243r^3 N_*^5}{2000\pi^2 \rho_*^2 R^3 K^3 T^3 \varepsilon^3}} \end{aligned} \quad (10)$$

We approximate that the cost c of large telescopes scales as $c \propto d^{2.5}$, (van Belle et al. 2004), and then we can say that the cost c can be expressed as

$$c = C d^{2.5} = C \left(4\text{SNR}_0 \sqrt[6]{\frac{243r^3 N_*^5}{2000\pi^2 \rho_*^2 R^3 K^3 T^3 \varepsilon^3} \eta_{\oplus}^{-5/6}} \right)^{5/2}$$

where C is a scaling constant for cost.

$$c = C \left(\frac{62208 \cdot r^3 \text{SNR}_0^6 \cdot N_*^5}{125\pi^2 \rho_*^2 T^3 R^3 K^3 \varepsilon^3} \right)^{5/12} \eta_{\oplus}^{-25/12} \quad (11)$$

Similar equations can be found for other cost-scaling exponents.

2.1.2. With advanced approximation

We now use the approximation derived in Appendix A:

$$\sum_{k=1}^{N_*} k^{2/3} \approx \frac{3(N_*+1)^{5/3}}{5} - \frac{(N_*+1)^{2/3}}{2} - \frac{1}{10} \quad (72)$$

This approximation has far lower error compared to the exact Riemann sum. So,

$$d^2 = \frac{16r\text{SNR}_0^2}{RKT \varepsilon} \left(\frac{3}{4\pi\rho_*} \right)^{2/3} \cdot \left(\frac{3(N_*+1)^{5/3}}{5} - \frac{(N_*+1)^{2/3}}{2} - \frac{1}{10} \right)$$

$$d = 4\sqrt{r}\text{SNR}_0 \left(\frac{9}{16\pi^2 \rho_*^2 R^3 K^3 T^3 \varepsilon^3} \right)^{1/6} \cdot \left(\frac{3(N_*+1)^{5/3}}{5} - \frac{(N_*+1)^{2/3}}{2} - \frac{1}{10} \right)^{1/2}$$

$$d = \left(\frac{2304r^3 \text{SNR}_0^6}{\pi^2 \rho_*^2 R^3 K^3 T^3 \varepsilon^3} \right)^{1/6} \cdot \left(\frac{3(N_*+1)^{5/3}}{5} - \frac{(N_*+1)^{2/3}}{2} - \frac{1}{10} \right)^{1/2} \quad (12)$$

Again, we use the approximation that cost scales as $d^{2.5}$, so the cost c is

$$c = C \left(\frac{2304r^3 \text{SNR}_0^6}{\pi^2 \rho_*^2 R^3 K^3 T^3 \varepsilon^3} \right)^{5/12} \cdot \left(\frac{3(N_\oplus/\eta_\oplus + 1)^{5/3}}{5} - \frac{(N_\oplus/\eta_\oplus + 1)^{2/3}}{2} - \frac{1}{10} \right)^{5/4} \quad (13)$$

Again, similar expressions can be found for different exponents for the scaling of cost with telescope diameter.

2.1.3. Solving for other variables

It may be useful to rearrange equation 10 to solve for different variables. A few rearrangements are given here.

$$N_\oplus = \eta_\oplus^5 \sqrt[5]{\frac{125d^6 \pi^2 \rho_*^2 R^3 K^3 T^3 \varepsilon^3}{62208 \text{SNR}_0^6 r^3}} \quad (14)$$

$$T = \sqrt[3]{\frac{62208 \text{SNR}_0^6 r^3 N_\oplus^5}{125d^6 \pi^2 \rho_*^2 R^3 K^3 \varepsilon^3 \eta_\oplus^5}} \quad (15)$$

2.2. With Precursor Knowledge

We now evaluate the benefits of precursor knowledge by extending the previously introduced basic yield model. In this section, we assume that the survey has perfect precursor knowledge from previous observations, and only serves to confirm the existence of and characterize the exo-Earths. The lack of consideration for inner working angle in the basic yield model is somewhat more appropriate here, because determination of the orbital ephemerides can be accomplished through the precursor observations; hence we can target the systems with exo-Earths when they are known to be exterior to the telescope's inner working angle. In other words, we assume that over the duration of the survey there is always at least one exo-Earth available to observe outside the inner working angle at any given time for at least one system in the target list, and over the course of the survey duration, all exo-Earth hosts will be targeted when the exo-Earth is exterior to the inner working angle. We revisit this assumption by explicitly considering the impact of an inner working angle in §3.

Since we now know which stars have target-able exo-Earths, our stellar sample size contains only exo-Earth hosting systems and matches the number of exo-Earths we wish to confirm and characterize, and thus $N_* = N_\oplus$. However, we aren't changing the density of the stars, only our selection process, so equation 2 still applies.

$$\rho_\oplus = \rho_* \eta_\oplus = \frac{N_\oplus}{\frac{4}{3}\pi D_{\text{lim}}^3} \quad (2)$$

Again, the total survey on-sky duration can be expressed as the sum of individual target exposures, again ignoring slew times and overhead:

$$\sum_{k=1}^{N_*} t_k = T$$

where t_k is the time spent on the k th star, and T is the total on-sky time. Again, the detected photo-electron rate from the k th exo-Earth is:

$$R_e = RK \frac{\pi(d/2)^2 \varepsilon}{4\pi D_k^2} = \frac{Rd^2 \varepsilon}{16D_k^2} \quad (3)$$

and the per-target observing time of:

$$t_k = \frac{r \text{SNR}_0^2}{R_e} = \frac{16r \text{SNR}_0^2 D_k^2}{RKd^2 \varepsilon} \quad (4)$$

We assume again that the stars are randomly distributed throughout a sphere of radius D_{lim} , and thus we can divide the sphere up into N_\oplus spherical shells of equal volume, and assume that there is exactly one star with an exo-Earth contained in each spherical shell. Each shell would have volume $\frac{4\pi}{3N_\oplus} D_{\text{lim}}^3$. Therefore, the outer radius of the k th spherical shell D_k must satisfy

$$\frac{4\pi}{3} D_k^3 = \frac{4k\pi}{3N_\oplus} D_{\text{lim}}^3 \quad (16)$$

$$D_k^3 = \frac{k}{N_\oplus} D_{\text{lim}}^3 = \frac{3kN_\oplus}{4\pi\rho_*\eta_\oplus N_\oplus} = \frac{3k}{4\pi\rho_*\eta_\oplus} \quad (17)$$

$$t_k = \frac{16r \text{SNR}_0^2 D_k^2}{RKd^2 \varepsilon} = \frac{16r \text{SNR}_0^2}{RKd^2 \varepsilon} \left(\frac{3k}{4\pi\rho_*\eta_\oplus} \right)^{2/3} \quad (18)$$

Because the total on-sky time must be equal to the sum of the integration times, again ignoring slew time and other overheads, we have:

$$T = \frac{16r \text{SNR}_0^2}{RKd^2 \varepsilon} \left(\frac{3}{4\pi\rho_*\eta_\oplus} \right)^{2/3} \sum_{k=1}^{N_\oplus} k^{2/3} \quad (19)$$

So, because T is fixed, we know that

$$d^2 = \frac{16r \text{SNR}_0^2}{RKT \varepsilon} \left(\frac{3}{4\pi\rho_*\eta_\oplus} \right)^{2/3} \sum_{k=1}^{N_\oplus} k^{2/3} \quad (20)$$

2.2.1. With simple approximation

Again, we approximate

$$\sum_{k=1}^{N_\oplus} k^{2/3} \approx \int_0^{N_\oplus} x^{2/3} dx = \frac{3}{5} N_\oplus^{5/3}. \quad (21)$$

Again, this has a high percent error for small values of N_{\oplus} , so we assume $N_{\oplus} \geq 100$. For small surveys, this might be an unreasonable assumption. So,

$$d^2 = \frac{16rSNR_0^2}{RKT\varepsilon} \left(\frac{3}{4\pi\rho_*\eta_{\oplus}} \right)^{2/3} \frac{3}{5} N_{\oplus}^{5/3} \quad (22)$$

$$d = 4SNR_0 \left(\frac{3}{4\pi\rho_*\eta_{\oplus}} \right)^{1/3} \sqrt{\frac{3rN_{\oplus}^{5/3}}{5RKT\varepsilon}} \quad (23)$$

Again, we assume that the cost $c \propto d^{2.5}$, but similar results can be shown for other exponents.

$$\begin{aligned} c &= C \left(4SNR_0 \left(\frac{3}{4\pi\rho_*\eta_{\oplus}} \right)^{1/3} \sqrt{\frac{3rN_{\oplus}^{5/3}}{5RKT\varepsilon}} \right)^{5/2} \\ c &= C \left(4SNR_0 \left(\frac{3}{4\pi\rho_*} \right)^{1/3} \sqrt{\frac{3rN_{\oplus}^{5/3}}{5RKT\varepsilon} \eta_{\oplus}^{-1/3}} \right)^{5/2} \\ c &= C \left(4SNR_0 \left(\frac{3}{4\pi\rho_*} \right)^{1/3} \sqrt{\frac{3rN_{\oplus}^{5/3}}{5RKT\varepsilon}} \right)^{5/2} \eta_{\oplus}^{-5/6} \\ c &= C \left(\frac{62208 \cdot r^3 SNR_0^6 N_{\oplus}^5}{125\pi^2 \rho_*^2 T^3 R^3 K^3 \varepsilon^3} \right)^{5/12} \eta_{\oplus}^{-5/6} \quad (24) \end{aligned}$$

2.2.2. With advanced approximation

Again, we use the approximation derived in [Appendix A](#):

$$\sum_{k=1}^{N_{\oplus}} k^{2/3} \approx \frac{3(N_{\oplus}+1)^{5/3}}{5} - \frac{(N_{\oplus}+1)^{2/3}}{2} - \frac{1}{10} \quad (72)$$

Note that we use N_{\oplus} instead of N_* to prevent confusion. So,

$$\begin{aligned} d^2 &= \frac{16rSNR_0^2}{RKT\varepsilon} \left(\frac{3}{4\pi\rho_*\eta_{\oplus}} \right)^{2/3} \cdot \\ &\quad \left(\frac{3(N_{\oplus}+1)^{5/3}}{5} - \frac{(N_{\oplus}+1)^{2/3}}{2} - \frac{1}{10} \right) \\ d &= 4\sqrt{r}SNR_0 \left(\frac{9}{16\pi^2\rho_*^2\eta_{\oplus}^2R^3K^3T^3\varepsilon^3} \right)^{1/6} \cdot \\ &\quad \left(\frac{3(N_{\oplus}+1)^{5/3}}{5} - \frac{(N_{\oplus}+1)^{2/3}}{2} - \frac{1}{10} \right)^{1/2} \\ d &= \left(\frac{2304r^3SNR_0^6}{\pi^2\rho_*^2R^3K^3T^3\varepsilon^3} \right)^{1/6} \cdot \\ &\quad \left(\frac{3(N_{\oplus}+1)^{5/3}}{5} - \frac{(N_{\oplus}+1)^{2/3}}{2} - \frac{1}{10} \right)^{1/2} \eta_{\oplus}^{-1/3} \quad (25) \end{aligned}$$

Again, we will be making the assumption that cost scales as $d^{2.5}$, so the cost c is

$$\begin{aligned} c &= C \left(\frac{2304r^3SNR_0^6}{\pi^2\rho_*^2R^3K^3T^3\varepsilon^3} \right)^{5/12} \cdot \\ &\quad \left(\frac{3(N_{\oplus}+1)^{5/3}}{5} - \frac{(N_{\oplus}+1)^{2/3}}{2} - \frac{1}{10} \right)^{5/4} \eta_{\oplus}^{-5/6} \quad (26) \end{aligned}$$

Again, similar expressions can be found for different exponents.

2.2.3. Solving for other variables

To solve for N_{\oplus} , we begin with equation 22:

$$d^2 = \frac{16rSNR_0^2}{RKT\varepsilon} \left(\frac{3}{4\pi\rho_*\eta_{\oplus}} \right)^{2/3} \frac{3}{5} N_{\oplus}^{5/3} \quad (22)$$

We rearrange the terms:

$$N_{\oplus} = \sqrt[5]{\frac{125\pi^2 d^6 R^3 K^3 T^3 \varepsilon^3 \rho_*^2 \eta_{\oplus}^2}{62208 r^3 SNR_0^6}} \quad (27)$$

To solve for SNR_0 in terms of the other variables, we begin with equation 23:

$$d = 4SNR_0 \left(\frac{3}{4\pi\rho_*\eta_{\oplus}} \right)^{1/3} \sqrt{\frac{3rN_{\oplus}^{5/3}}{5RKT\varepsilon}} \quad (23)$$

We rearrange the equation and simplify.

$$SNR_0 = \sqrt[3]{\frac{4\pi\rho_*\eta_{\oplus}}{3}} \sqrt{\frac{5RKT\varepsilon d^2}{48rN_{\oplus}^{5/3}}} \quad (28)$$

To solve for T , we begin with equation 19.

$$T = \frac{16rSNR_0^2}{RKd^2\varepsilon} \left(\frac{3}{4\pi\rho_*\eta_{\oplus}} \right)^{2/3} \sum_{k=1}^{N_{\oplus}} k^{2/3} \quad (19)$$

We again approximate $\sum_{k=1}^{N_{\oplus}} k^{2/3} \approx \frac{3}{5} N_{\oplus}^{5/3}$:

$$T = \frac{48rSNR_0^2 N_{\oplus}^{5/3}}{5RKd^2\varepsilon} \left(\frac{3}{4\pi\rho_*\eta_{\oplus}} \right)^{2/3} \quad (29)$$

3. PHOTON NOISE YIELD MODEL ACCOUNTING FOR IWA

Now we introduce a more complicated model, in which we account for how the inner working angle impacts the target exposure times. In order to model the impact of the inner working angle on yield, one might scale the required on-sky

time for each exo-Earth inversely by the “time fraction usable,” the percentage of time that the exo-Earth spends outside of the telescope’s inner working angle, as a function of that each individual exo-Earth’s inclination. Such a case-by-case scaling for individual exo-Earth inclinations would not yield a simple analytic approximation for the total survey duration. Instead, we average the time fraction usable of the exo-Earth over all inclinations assuming uniform random distribution in the cosine of the inclination. Then, we scale the total on-sky time inversely by that average, to obtain an approximation of the time needed to achieve the required yield in an uninformed survey. For some targets, with face-on inclinations the required time will be shorter than average (a larger fraction of the time the target will be outside the iwa), whereas for edge-on targets the required time will be longer than average (a smaller fraction of the time the target will be outside the iwa).

We make some additional simplifications and assumptions. Again, we do not account for variable spectral types, or distances of the exo-Earths from their host stars – we assume all exo-Earths orbit at 1 au from a Sun-like star. We also do not account for revisits in our analysis at different orbital phases. We also assume that only a survey with precursor knowledge can wait for the right time to target a given exo-Earth when it is outside the iwa , whereas an uninformed survey will sometimes observe a system when the exo-Earth is inside the iwa .

Finally, while we continue to assume that the target stars are uniformly distributed in a spherical volume with radius D_{lim} in calculating exposure times, for assessing the impact of the iwa , we instead assume that all planets are at D_{lim} , a worst case scenario in assessing the fraction of time a given exo-Earth is external to the iwa . Scaling this iwa impact with D_k instead of D_{lim} does not yield an analytic sum for the survey duration, although this can be computed numerically, which we next show.

3.1. No Precursor Knowledge

An uninformed survey will be forced to target potential exo-Earths randomly in orbital phase, without any initial knowledge of their orbital ephemerides. Thus, the efficiency of observations would be proportional to the average percentage of time in which the planet is observable. Because we are considering the impact of the inner working angle, we assume that the planet is observable when outside the telescope’s inner working angle, and unobservable other times. Note, the same is not true for revisits, which are not considered herein, but will asymptote to the precursor knowledge case as the orbital ephemerides are constrained and thus observations can be optimally timed after the initial detection and with improvements in orbital determination.

As before, $T = \sum_{k=1}^{N_*} t_k$. Because some fraction of that time t_k is unusable (e.g. when the planet is inside the iwa), we can

express it as $t_k = u_k + w_k$, where u_k is the usable time, and w_k is the unusable time. We have an expression for how much usable time we need:

$$u_k = \frac{16rSNR_0^2}{RKd^2\varepsilon} \left(\frac{3k}{4\pi\rho_*} \right)^{2/3} \quad (5)$$

As derived in [Appendix B](#), the fraction of time usable for a given exoplanet can be expressed as the piecewise function

$$t_f = \begin{cases} 0 & s_c \geq a \\ \frac{2}{\pi} \cdot \arccos \left(\frac{1}{a} \cdot \sqrt{\frac{iwa^2 - a^2 \cos^2 i}{1 - (\cos^2 i)}} \right) & a \cos i < s_c < a \\ 1 & a \cos i > s_c \end{cases}$$

where a is the exo-Earth’s semi-major axis, $s_c = D_k \cdot iwa$ is the projection of the inner working angle at the distance to the target star (we assume the sphere centered on the observer and intersecting the star to be tangentially flat, such that a flat projection may be assumed), and $\cos i$ is the cosine of the inclination.

Because $\cos i$ is uniform random, the average time fraction usable can be obtained by integrating the expression above $d \cos i$ from 0 to 1. That yields the equation

$$t_a = \frac{\sqrt{a^2 - s_c^2}}{a} \quad (75)$$

where t_a is the average time fraction usable.

We can say that, on average

$$t_k = \frac{u_k}{t_a} = \frac{a}{\sqrt{a^2 - s_c^2}} \cdot \frac{16rSNR_0^2}{RKd^2\varepsilon} \left(\frac{3k}{4\pi\rho_*} \right)^{2/3} \quad (30)$$

We note that the average time spent observing a target for which an exoplanet is outside the iwa is a simplifying assumption - e.g. that we are uniform randomly observing this target in time, as opposed to observing this target with a cadence that maximizes the probability that the planet is captured outside the iwa . This is thus a bounding worst-case scenario.

To solve for d , we recall that $s_c = D_k \cdot iwa$. However, substituting this in Equation 30 and summing over all the targets results in a non-trivial summation in k :

$$T = \frac{16rSNR_0^2}{RKd^2\varepsilon} \left(\frac{3}{4\pi\rho_*} \right)^{1/3} \sum_{k=1}^{N_*} \frac{k^{1/3}}{\sqrt{\left(\frac{4\pi\rho_*}{3k} \right)^{2/3} - \left(\frac{iwa}{a} \right)^2}} \quad (31)$$

Instead, we assume a worst-case scenario – in correcting for the average fraction of the time that the planet is external to the inner working angle, we assume that all the exo-Earths are at the survey limiting distance D_{lim} and thus $s_c = D_{\text{lim}} \cdot iwa$ is independent of k . Alternatively, we could have taken the

average distance, $\langle D_k \rangle = 2^{-1/3} D_{\text{lim}} \sim 0.79 D_{\text{lim}}$. Next, we approximate (Mawet et al. 2012)

$$\text{iwa} \approx \frac{n_i \lambda}{d} \text{ rad} \quad (32)$$

for some $n_i \approx 3$. Then we have from Equation 30:

$$T = \frac{16rSNR_0^2 a}{RKd^2 \varepsilon \sqrt{a^2 - s_c^2}} \left(\frac{3}{4\pi\rho_*} \right)^{2/3} \sum_{k=1}^{N_*} k^{2/3}$$

$$T = \frac{16rSNR_0^2}{RKd^2 \varepsilon \sqrt{1 - \left(\frac{s_c}{a}\right)^2}} \left(\frac{3}{4\pi\rho_*} \right)^{2/3} \sum_{k=1}^{N_*} k^{2/3} \quad (33)$$

$$T = \frac{16rSNR_0^2}{RK\varepsilon d^2 \sqrt{1 - \left(\frac{n_i D_{\text{lim}} \lambda}{ad}\right)^2}} \left(\frac{3}{4\pi\rho_*} \right)^{2/3} \sum_{k=1}^{N_*} k^{2/3} \quad (34)$$

which has a more trivial summation in k and is independent of η_{\oplus} . From the above, T diverges as d approaches $\frac{3D_{\text{lim}}\lambda}{a}$. This is as expected – planets with semi-major axes approaching the inner working angle have a fraction of time observable outside the inner working angle that limits to zero. We discuss the impact of this in 5.1.

Next, for simplification of presentation, we define:

$$n \equiv \frac{n_i \lambda}{a} \quad (35)$$

$$m \equiv \frac{16rSNR_0^2}{RK\varepsilon} \left(\frac{3}{4\pi\rho_*} \right)^{2/3} \quad (36)$$

Where λ is the wavelength at which we are observing. Note that neither m nor n has any dependence on η_{\oplus} . Then,

$$T = \frac{m}{d^2 \sqrt{1 - \left(\frac{D_{\text{lim}} n}{d}\right)^2}} \sum_{k=1}^{N_*} k^{2/3} \quad (37)$$

The solution to this, as derived in Appendix C, is

$$d = \pm \sqrt{\frac{D_{\text{lim}}^2 n^2}{2} \pm \frac{1}{2} \sqrt{D_{\text{lim}}^4 n^4 + \frac{4m^2 \left(\sum_{k=1}^{N_*} k^{2/3}\right)^2}{T^2}}} \quad (38)$$

We can remove some common factors:

$$d = \pm \frac{D_{\text{lim}} n}{\sqrt{2}} \sqrt{1 \pm \sqrt{1 + \frac{4m^2 \left(\sum_{k=1}^{N_*} k^{2/3}\right)^2}{D_{\text{lim}}^4 n^4 T^2}}}$$

The diameter can't be negative, so we can eliminate the negative solutions:

$$d = \frac{D_{\text{lim}} n}{\sqrt{2}} \sqrt{1 \pm \sqrt{1 + \frac{4m^2 \left(\sum_{k=1}^{N_*} k^{2/3}\right)^2}{D_{\text{lim}}^4 n^4 T^2}}}$$

Also, the inner square root contains 1 plus some non-negative number, so the result of the inner square root is at least 1. Evaluating the $-$ of the \pm for the outer square root would require taking the square root of a negative number, which would result in a complex diameter. The telescope diameter must be a real number, so we can eliminate the $-$ case. Thus,

$$d = \frac{D_{\text{lim}} n}{\sqrt{2}} \sqrt{1 + \sqrt{1 + \frac{4m^2 \left(\sum_{k=1}^{N_*} k^{2/3}\right)^2}{D_{\text{lim}}^4 n^4 T^2}}} \quad (39)$$

3.1.1. With simple Approximation

Again, we assume that

$$\sum_{k=1}^{N_*} k^{2/3} \approx \int_0^{N_*} x^{2/3} dx = \frac{3}{5} N_*^{5/3} \quad (8)$$

Again, this has a percent error $>0.83\%$ for values of $N_* < 100$, so we assume $N_* \geq 100$. Substituting that in,

$$d = \frac{D_{\text{lim}} n}{\sqrt{2}} \sqrt{1 + \sqrt{1 + \frac{4m^2 \left(\frac{3}{5} N_*^{5/3}\right)^2}{D_{\text{lim}}^4 n^4 T^2}}}$$

$$d = \frac{D_{\text{lim}} n}{\sqrt{2}} \sqrt{1 + \sqrt{1 + \frac{36m^2 N_*^{10/3}}{25D_{\text{lim}}^4 n^4 T^2}}} \quad (40)$$

Because

$$N_* = \frac{4\pi\rho_* D_{\text{lim}}^3}{3}, \quad (1)$$

we can split up the $N_*^{10/3}$ into $N_*^2 \cdot N_*^{4/3}$, and cancel out the factors of D_{lim} :

$$d = \frac{D_{\text{lim}} n}{\sqrt{2}} \sqrt{1 + \sqrt{1 + \frac{36m^2 N_*^2}{25n^4 T^2} \cdot \frac{N_*^{4/3}}{D_{\text{lim}}^4}}}$$

$$d = \frac{D_{\text{lim}} n}{\sqrt{2}} \sqrt{1 + \sqrt{1 + \frac{36m^2 N_*^2}{25n^4 T^2} \left(\frac{4\pi\rho_*}{3}\right)^{4/3}}} \quad (41)$$

To substitute back in for our simplifying variable m^2 , we square equation 36:

$$m^2 = \frac{256r^2 SNR_0^4}{R^2 K^2 \varepsilon^2} \left(\frac{3}{4\pi\rho_*} \right)^{4/3}$$

to get:

$$d = \frac{D_{\text{lim}} n}{\sqrt{2}} \sqrt{1 + \sqrt{1 + \frac{36 \cdot 256r^2 SNR_0^4 N_*^2}{25R^2 K^2 \varepsilon^2 n^4 T^2} \left(\frac{3 \cdot 4\pi\rho_*}{3 \cdot 4\pi\rho_*}\right)^{4/3}}}$$

which simplifies to:

$$d = \frac{D_{\text{lim}} n}{\sqrt{2}} \sqrt{1 + \sqrt{1 + \frac{9216r^2 \text{SNR}_0^4 N_*^2}{25R^2 K^2 \varepsilon^2 n^4 T^2}}} \quad (42)$$

To find the η_{\oplus} dependence, we can expand N_* and D_{lim} :

$$d = \frac{n}{\sqrt{2}} \sqrt[3]{\frac{3N_{\oplus}}{4\pi\rho_*\eta_{\oplus}}} \sqrt{1 + \sqrt{1 + \frac{9216r^2 \text{SNR}_0^4 N_{\oplus}^2}{25R^2 K^2 \varepsilon^2 n^4 T^2 \eta_{\oplus}^2}}} \quad (43)$$

To find the cost, we again assume $c = Cd^{2.5}$:

$$c = C \left(\frac{n}{\sqrt{2}} \sqrt[3]{\frac{3N_{\oplus}}{4\pi\rho_*\eta_{\oplus}}} \sqrt{1 + \sqrt{1 + \frac{9216r^2 \text{SNR}_0^4 N_{\oplus}^2}{25R^2 K^2 \varepsilon^2 n^4 T^2 \eta_{\oplus}^2}}} \right)^{5/2} \quad (44)$$

where

$$n = \frac{n_i \lambda}{a} \quad (45)$$

As before, a better approximation can be derived using a more accurate finite summation for $k^{2/3}$, as done in earlier sections, which we do not explicitly carry out herein.

3.1.2. Solving for other variables

To solve for N_{\oplus} , we begin with equation 37:

$$T = \frac{m}{d^2 \sqrt{1 - \left(\frac{D_{\text{lim}} n}{d}\right)^2}} \sum_{k=1}^{N_*} k^{2/3} \quad (37)$$

We substitute the definition for D_{lim} found in equation 1, and again approximate $\sum_{k=1}^{N_*} k^{2/3} \approx \frac{3}{5} N_*^{5/3}$.

$$T \approx \frac{3mN_*^{5/3}}{5d^2 \sqrt{1 - \left(\frac{3N_* n^3}{4\pi\rho_* d^3}\right)^{2/3}}} \quad (45)$$

The only term with any N_{\oplus} dependence is $N_* = N_{\oplus}/\eta_{\oplus}$. To simplify the presentation of our solution, we define:

$$\alpha \equiv \frac{5Td^2}{3m}$$

$$\beta \equiv \frac{n^2}{d^2} \left(\frac{3}{4\pi\rho_*} \right)^{2/3}$$

Then, the above equation could be rewritten as

$$\alpha = \frac{N_*^{5/3}}{\sqrt{1 - \beta N_*^{2/3}}} \quad (46)$$

We square to eliminate the square root, and rearrange.

$$\alpha^2 = \frac{N_*^{10/3}}{1 - \beta N_*^{2/3}}$$

$$\alpha^2 - \alpha^2 \beta N_*^{2/3} = N_*^{10/3}$$

$$N_*^{10/3} + \alpha^2 \beta N_*^{2/3} - \alpha^2 = 0 \quad (47)$$

N_* is the positive real root of this polynomial which can be computed numerically, and $N_{\oplus} = \eta_{\oplus} N_*$ may be derived from N_* .

To solve for SNR_0 , we begin with equation 34:

$$T = \frac{16r \text{SNR}_0^2}{RK\varepsilon d^2 \sqrt{1 - \left(\frac{n_i D_{\text{lim}} \lambda}{ad}\right)^2}} \left(\frac{3}{4\pi\rho_*} \right)^{2/3} \sum_{k=1}^{N_*} k^{2/3} \quad (34)$$

We approximate $\sum_{k=1}^{N_*} k^{2/3} \approx \frac{3}{5} N_*^{5/3}$:

$$T = \frac{48r \text{SNR}_0^2 N_*^{5/3}}{5RK\varepsilon d^2 \sqrt{1 - \left(\frac{n_i D_{\text{lim}} \lambda}{ad}\right)^2}} \left(\frac{3}{4\pi\rho_*} \right)^{2/3}$$

We rearrange the equation.

$$\text{SNR}_0^2 = \frac{5RK T \varepsilon d^2 \sqrt{1 - \left(\frac{n_i D_{\text{lim}} \lambda}{ad}\right)^2}}{48r N_*^{5/3}} \left(\frac{4\pi\rho_*}{3} \right)^{2/3}$$

And we take a square root.

$$\text{SNR}_0 = \sqrt{\frac{5RK T \varepsilon d^2 \sqrt{1 - \left(\frac{n_i D_{\text{lim}} \lambda}{ad}\right)^2}}{48r N_*^{5/3}}} \sqrt[3]{\frac{4\pi\rho_*}{3}} \quad (48)$$

3.2. Precursor Knowledge

Next, we assume we have precursor knowledge of the stars that possess Earth-sized exoplanets in their Habitable Zones, and precursor knowledge of their orbital ephemerides (e.g. period and orbital phase), modulo an unknown inclination. This is thus a bounding best-case scenario. With an unknown inclination, there is still an unknown fraction of time that the exo-Earth is inside the iwa, and thus the planet may not be observable at all phases (unless $a \cos i > s_c$). However, the planet can be observed at quadrature. The planet will always be outside the iwa at quadrature, provided the telescope diameter is adequate (e.g. $a > s_c$). Thus this scenario reduces to assessing the number of stars for which the condition $a > s_c$ is satisfied.

We can assume that we can target a given exoplanet host star at a time such that the exo-Earth is guaranteed to be observable and located exterior to the observatory iwa, modulo the unknown inclination. We will also assume for simplicity that mission observations can be scheduled so that each exoplanet is targeted at quadrature, and that there is always a planet available to target at quadrature. Further, if there are two planets at quadrature at the same over-lapping time, we assume one planet's observations can be deferred to a subsequent orbit without extending the mission lifetime.

Observing the exo-Earth at quadrature will not constrain the inclination of the exo-Earth orbit significantly, and thus an additional observation will be required to constrain the inclination. Thus we can assume a minimum of two visits per planet would be required in this scenario, but this would also be true of all the other scenarios considered herein.

Because of the targeted observations, no time will be lost due to bad timing (observing when the planet is inside the *iwa*). Consequently, as long as photon noise is the limiting factor for the telescope diameter, it should be the same as was derived in section §2.2.

Using the simpler approximation,

$$c = C \left(\frac{62208 \cdot r^3 \text{SNR}_0^6 N_\oplus^5}{125 \pi^2 \rho_*^2 T^3 R^3 K^3 \varepsilon^3} \right)^{5/12} \eta_\oplus^{-5/6}$$

Note that the equation for total on-sky time is the same as before:

$$T = \frac{48r\text{SNR}_0^2 N_\oplus^{5/3}}{5RKd^2\varepsilon} \left(\frac{3}{4\pi\rho_*\eta_\oplus} \right)^{2/3} \quad (49)$$

This establishes an upper bound on the survey yield, for a given total on-sky time:

$$\begin{aligned} N_\oplus^{5/3} &= \left(\frac{4\pi\rho_*\eta_\oplus}{3} \right)^{2/3} \frac{5RKTd^2\varepsilon}{48r\text{SNR}_0^2} \\ N_\oplus^5 &= \left(\frac{4\pi\rho_*\eta_\oplus}{3} \right)^2 \frac{125R^3K^3T^3d^6\varepsilon^3}{110592r^3\text{SNR}_0^6} \\ N_\oplus &= \sqrt[5]{\frac{125\pi^2\rho_*^2\eta_\oplus^2R^3K^3T^3d^6\varepsilon^3}{62208r^3\text{SNR}_0^6}} \quad (50) \end{aligned}$$

Similarly, we can establish a minimum telescope diameter.

$$d = \left(\frac{3}{4\pi\rho_*\eta_\oplus} \right)^{1/3} \sqrt{\frac{48r\text{SNR}_0^2 N_\oplus^{5/3}}{5RKT\varepsilon}} \quad (51)$$

Similar expressions can be found using the more advanced approximation derived in [Appendix A](#):

$$\begin{aligned} c &= C \left(\frac{2304r^3\text{SNR}_0^6}{\pi^2\rho_*^2R^3K^3T^3\varepsilon^3} \right)^{5/12} \\ &\quad \left(\frac{3(N_\oplus+1)^{5/3}}{5} - \frac{(N_\oplus+1)^{2/3}}{2} - \frac{1}{10} \right)^{5/4} \eta_\oplus^{-5/6} \end{aligned}$$

4. INNER WORKING ANGLE LIMITED YIELD MODEL

The requirement that all Exo-Earths must have a projected semi-major axis greater than the telescope's projected inner working angle ($a > s_c$) creates a hard lower bound for the telescope diameter, which is referred to as the “*iwa* limited” regime. In some situations, this lower bound is greater than the diameter otherwise required by photon noise limited regime as we have explored in §2 and §3. In this section,

we seek to derive an expression for the telescope diameter in such an *iwa* limited scenario. Note that this expression is applicable to both precursor and no-precursor knowledge cases; precursor knowledge has no impact on this requirement.

To evaluate the requirement that $a > s_c$ for all of our target stars, we examine the definition that we set out in [Appendix B](#):

$$s_c = D_{\text{lim}} \cdot iwa \quad (73)$$

In order to satisfy our requirement, this must be less than a , the semi-major axis of the exo-Earth, determined by the position of the habitable zone for that star. Because we are primarily considering solar analogues in our toy model, $a \sim 1$ au.

Again, we approximate

$$iwa \approx \frac{n_i\lambda}{d} \text{ rad}, \quad (32)$$

where λ is the observational wavelength. So,

$$s_c = \frac{n_i D_{\text{lim}} \lambda}{d}. \quad (52)$$

In order to satisfy the condition, s_c must be at least

$$s_c = \frac{n_i D_{\text{lim}} \lambda}{d} = a.$$

Solving for d , we get

$$d = \frac{n_i D_{\text{lim}} \lambda}{a}. \quad (53)$$

Substituting D_{lim} in terms of η_\oplus :

$$d = \frac{n_i\lambda}{a} \sqrt[3]{\frac{3N_\oplus}{4\pi\rho_*\eta_\oplus}} = \frac{n_i\lambda}{a} \sqrt[3]{\frac{3N_\oplus}{4\pi\rho_*} \eta_\oplus^{-1/3}} \quad (54)$$

This is the minimum value for d , based on the inner working angle. Note that this expression applies to situations with and without precursor knowledge.

Again assuming that the cost $c = Cd^{2.5}$,

$$c = C \left(\frac{n_i\lambda}{a} \sqrt{\frac{3N_\oplus}{4\pi\rho_*}} \right)^{2.5} \eta_\oplus^{-5/6} \quad (55)$$

4.1. No Precursor Knowledge

If we assume the telescope diameter is defined by Equation 54 in the inner working angle limited regime, we next derive the total on-sky time required by this survey. Only our diameter has changed, so the target scheduling is still the same. The equation for T , then, is the same as before in §3.1:

$$T = \frac{16r\text{SNR}_0^2}{RK\varepsilon d^2 \sqrt{1 - \left(\frac{n_i D_{\text{lim}} \lambda}{ad} \right)^2}} \left(\frac{3}{4\pi\rho_*} \right)^{2/3} \sum_{k=1}^{N_*} k^{2/3} \quad (34)$$

Again, we have that the survey duration diverges as $d \rightarrow \frac{n_i D_{\text{lim}} \lambda}{a}$ and the survey duration is a worst-case scenario under the assumption that all planets are located at $D_k \rightarrow D_{\text{lim}}$ for estimating the fraction of survey time a given target is located outside the *iwa*.

4.2. Precursor Knowledge

Since only our expression for the minimum telescope diameter has changed, our total on-sky time is the same:

$$T = \frac{16rSNR_0^2}{RKd^2\varepsilon} \left(\frac{3}{4\pi\rho_*\eta_\oplus} \right)^{2/3} \sum_{k=1}^{N_\oplus} k^{2/3} \quad (19)$$

Substituting $d = \frac{n_i D_{\text{lim}} \lambda}{a}$, the minimum telescope diameter required for the most distant target to have a planet external to the *iwa*:

$$T = \frac{16rSNR_0^2 a^2}{n_i^2 RK \varepsilon D_{\text{lim}}^2 \lambda^2} \left(\frac{3}{4\pi\rho_*\eta_\oplus} \right)^{2/3} \sum_{k=1}^{N_\oplus} k^{2/3} \quad (56)$$

We use the simple approximation $\sum_{k=1}^{N_\oplus} k^{2/3} \approx \frac{3}{5} N_\oplus^{5/3}$:

$$T = \frac{48rSNR_0^2 a^2 N_\oplus^{5/3}}{5n_i^2 RK \varepsilon D_{\text{lim}}^2 \lambda^2} \left(\frac{3}{4\pi\rho_*\eta_\oplus} \right)^{2/3} \quad (57)$$

We substitute the definition of D_{lim} found by rearranging equation 2 and simplifying:

$$T = \frac{48rSNR_0^2 a^2 N_\oplus}{5n_i^2 RK \varepsilon \lambda^2} \quad (58)$$

which has a linear dependence with N_\oplus .

4.2.1. Solving for other variables

We rearrange equation 54 to solve for N_\oplus and η_\oplus . The maximum N_\oplus for a given set of parameters that satisfies $a > s_c$ is:

$$N_\oplus < \frac{4\pi\rho_*\eta_\oplus a^3 d^3}{3n_i^3 \lambda^3} \quad (59)$$

and the minimum necessary η_\oplus for a given set of parameters that satisfies $a > s_c$ is:

$$\eta_\oplus > \frac{3n_i^3 \lambda^3 N_\oplus}{4\pi\rho_* a^3 d^3} \quad (60)$$

5. WHEN ARE WE IWA LIMITED VERSUS PHOTON NOISE LIMITED IN OUR TELESCOPE DIAMETER?

Up until this point, we have estimated the required minimum telescope diameters and survey durations for a set of simplified direct imaging mission parameters, first considering when we are limited by photon noise in §2 and §3, and second when we are limited by inner working angle in §4, both with and without precursor knowledge. We now derive the transition between these two regimes to arrive at a prescription to determine when and under what combination of assumed mission parameters a direct imaging survey is photon noise or inner working angle limited.

5.1. No Precursor Knowledge

When we are limited by photon noise, including time lost due to unlucky timing when a planet is inside the *iwa*, the necessary diameter is

$$d_{\text{noise}} = \frac{D_{\text{lim}} n}{\sqrt{2}} \sqrt{1 + \sqrt{1 + \frac{36m^2 N_*^{10/3}}{25D_{\text{lim}}^4 n^4 T^2}}} \quad (40)$$

When we are limited by the inner working angle,

$$d_{\text{iwa}} = \frac{n_i D_{\text{lim}} \lambda}{a} \quad (53)$$

At the intersection, they must be equal.

$$\frac{n_i D_{\text{lim}} \lambda}{a} = \frac{D_{\text{lim}} n}{\sqrt{2}} \sqrt{1 + \sqrt{1 + \frac{36m^2 N_*^{10/3}}{25D_{\text{lim}}^4 n^4 T^2}}}$$

Substituting the first $n = \frac{n_i \lambda}{a}$:

$$\frac{n_i D_{\text{lim}} \lambda}{a} = \frac{n_i D_{\text{lim}} \lambda}{a \sqrt{2}} \sqrt{1 + \sqrt{1 + \frac{36m^2 N_*^{10/3}}{25D_{\text{lim}}^4 n^4 T^2}}}$$

We cancel the common factors and multiply by $\sqrt{2}$:

$$\sqrt{2} = \sqrt{1 + \sqrt{1 + \frac{36m^2 N_*^{10/3}}{25D_{\text{lim}}^4 n^4 T^2}}}$$

This results in the trivial expression that:

$$0 = \frac{36m^2 N_*^{10/3}}{25D_{\text{lim}}^4 n^4 T^2}$$

Recall that

$$N_* = \frac{4\pi\rho_* D_{\text{lim}}^3}{3} \quad (1)$$

Again, we split up $N_*^{10/3}$ into $N_*^2 \cdot N_*^{4/3}$, and cancel the factors of D_{lim} :

$$\frac{36m^2 N_*^2}{25n^4 T^2} \left(\frac{4\pi\rho_*}{3} \right)^{4/3} = 0$$

Again, we substitute in for m^2 and n^4 , take the square root and simplify:

$$\frac{rSNR_0^2 N_\oplus a^2}{RK \varepsilon T n_i^2 \lambda^2 \eta_\oplus} = 0 \quad (61)$$

This condition is met under a few possible trivial scenarios:

$$\left\{ \begin{array}{ll} SNR_0 = 0 & \text{We don't have to collect any photons.} \\ N_{\oplus} = 0 & \text{The survey yield is zero.} \\ a = 0 & \text{The targets are impossible to observe.} \\ RK\varepsilon T = \infty & \text{We collect infinite photons, so the photon noise requirement is meaningless.} \\ n_i^2 \lambda^2 = \infty & \text{The inner working angle is infinite.} \end{array} \right.$$

Thus, we conclude that a survey without precursor knowledge will always be limited by photon noise except in the trivial cases noted. In other words, photon noise considerations impose a larger minimum diameter requirement than the *iwa*. This may seem to be a counter-intuitive result at first: one can posit an “impossible” scenario where a small telescope diameter d with a large *iwa* can still collect the necessary number of photons given sufficient time to image an exo-Earth, but will traditionally be considered *iwa*-limited and unable to image close-in planets that are always inside the *iwa*. However, our photon-noise model treatment accounts for the observing time lost when the exo-Earth is inside the *iwa*, which drives up the observation time required and consequently the minimum telescope diameter. In this sense, our photon noise model already includes the impact of the *iwa* constraint, leading to this trivial equality. This also means that the previous result for T diverging in section 4.1 is irrelevant, because the situation in question never occurs – the photon noise model will always require a larger telescope diameter – and this situation of a diverging survey duration is in sense the “impossible” posited scenario.

5.2. Precursor Knowledge

In the case where we have precursor knowledge, when we are limited by photon noise, the necessary minimum diameter is given by:

$$d_{\text{noise}} = 4SNR_0 \left(\frac{3}{4\pi\rho_*\eta_{\oplus}} \right)^{1/3} \sqrt{\frac{3rN_{\oplus}^{5/3}}{5RKT\varepsilon}} \quad (23)$$

Note that we use the simple approximation for the summation over k .

When we are limited by the inner working angle constraint,

$$d_{\text{iwa}} = \frac{n_i D_{\text{lim}} \lambda}{a} \quad (53)$$

At an intersection between the photon noise and *iwa* regimes, both d -values must be equal.

Let us consider when the situation is limited by the inner working angle constraint. Then,

$$d_{\text{iwa}} > d_{\text{noise}}$$

$$\frac{n_i D_{\text{lim}} \lambda}{a} > 4SNR_0 \left(\frac{3}{4\pi\rho_*\eta_{\oplus}} \right)^{1/3} \sqrt{\frac{3rN_{\oplus}^{5/3}}{5RKT\varepsilon}}. \quad (62)$$

We rearrange the inequality, for $N_{\oplus} > 0$:

$$\frac{n_i \lambda}{a} \sqrt{\frac{5RKT\varepsilon}{3rN_{\oplus}^{5/3}}} D_{\text{lim}} > 4SNR_0 \left(\frac{3}{4\pi\rho_*\eta_{\oplus}} \right)^{1/3}$$

Because cubing preserves order, we cube both sides:

$$\left(\frac{n_i \lambda}{a} \sqrt{\frac{5RKT\varepsilon}{3rN_{\oplus}^{5/3}}} \right)^3 D_{\text{lim}}^3 > \frac{48SNR_0^3}{\pi\rho_*\eta_{\oplus}}$$

We can expand D_{lim} :

$$\left(\frac{n_i \lambda}{a} \sqrt{\frac{5RKT\varepsilon}{3rN_{\oplus}^{5/3}}} \right)^3 \frac{3N_{\oplus}}{4\pi\rho_*\eta_{\oplus}} > \frac{48SNR_0^3}{\pi\rho_*\eta_{\oplus}}$$

Because η_{\oplus} , ρ_* , and π are all positive, we can multiply by $\frac{4}{3}\pi\rho_*\eta_{\oplus}$:

$$\left(\frac{n_i \lambda}{a} \sqrt{\frac{5RKT\varepsilon}{3rN_{\oplus}^{5/3}}} \right)^3 N_{\oplus} > 64SNR_0^3$$

A cube root also preserves order, so we can take the cube root and simplify:

$$\frac{n_i \lambda}{a} \sqrt{\frac{5RKT\varepsilon}{3rN_{\oplus}^{5/3}}} N_{\oplus}^{1/3} > 4SNR_0$$

$$\frac{n_i \lambda}{a} \sqrt{\frac{5RKT\varepsilon}{3rN_{\oplus}}} > 4SNR_0$$

Squaring preserves order over all non-negative numbers, and both sides of this inequality are defined to be positive, so we can square both sides and rearrange:

$$\begin{aligned} \left(\frac{n_i \lambda}{a} \right)^2 \frac{5RKT\varepsilon}{3N_{\oplus}} &> 16rSNR_0^2 \\ \frac{n_i^2 \lambda^2}{a^2} \frac{5RKT\varepsilon}{3N_{\oplus}} &> 16rSNR_0^2 \\ \frac{5n_i^2 \lambda^2 RKT\varepsilon}{48rSNR_0^2 a^2} &> N_{\oplus} \end{aligned} \quad (63)$$

So, we are limited by the inner working angle for all N_{\oplus} such that

$$N_{\oplus} < \frac{5n_i^2 \lambda^2 RKT\varepsilon}{48rSNR_0^2 a^2}$$

Similarly, we are limited by photon noise for all N_{\oplus} such that

$$N_{\oplus} > \frac{5n_i^2 \lambda^2 RKT\varepsilon}{48rSNR_0^2 a^2}$$

and the intersection between the inner working angle and photon noise limited regimes occurs when

$$N_{\oplus} = \frac{5n_i^2 \lambda^2 RKT\varepsilon}{48rSNR_0^2 a^2} \quad (64)$$

6. RESULTS

6.1. Key Equations Summary

Herein we summarize our key results in deriving the dependence of the minimum telescope diameter on the mission parameter variables under study, given our assumptions. For a direct imaging survey without precursor knowledge, the minimum telescope diameter able to achieve the required yield is

$$d = \frac{n}{\sqrt{2}} \sqrt[3]{\frac{3N_{\oplus}}{4\pi\rho_*\eta_{\oplus}}} \sqrt{1 + \sqrt{1 + \frac{9216r^2SNR_0^4N_{\oplus}^2}{25R^2K^2\varepsilon^2n^4T^2\eta_{\oplus}^2}}} \quad (43)$$

Where $n \equiv n_i\lambda/a$.

For a direct imaging survey with perfect precursor knowledge, the minimum telescope diameter necessary to satisfy the photon noise requirement for a given yield is

$$d = 4SNR_0 \left(\frac{3}{4\pi\rho_*\eta_{\oplus}} \right)^{1/3} \sqrt{\frac{3rN_{\oplus}^{5/3}}{5RKT\varepsilon}} \quad (23)$$

The minimum telescope diameter necessary to satisfy the inner working angle requirement is

$$d = \frac{n_i\lambda}{a} \sqrt[3]{\frac{3N_{\oplus}}{4\pi\rho_*\eta_{\oplus}}} \quad (54)$$

Solving for the dependence on other variables besides telescope diameter are derived above and not repeated here.

6.2. When are we limited by iwa angle?

For no precursor knowledge, the minimum telescope diameter required is always driven by the photon noise requirement, when accounting for time lost due observations taken when the planet is inside the *iwa*, except in trivial situations. In the case of perfect precursor knowledge, the minimum telescope diameter required is limited by the inner working angle requirement when

$$\frac{5n_i^2\lambda^2RKT\varepsilon}{48rSNR_0^2a^2} > N_{\oplus} \quad (63)$$

Conversely, the minimum telescope diameter is limited by the photon noise requirement when

$$\frac{5n_i^2\lambda^2RKT\varepsilon}{48rSNR_0^2a^2} < N_{\oplus}$$

7. DISCUSSION

We have derived simplified analytic expressions and scaling relations for the telescope diameter as a function of key direct imaging mission parameters such as the occurrence rate of Exo-Earths, the mission yield, survey duration, and

other mission properties. We simplified our analytic treatment by assuming identical Sun-like stars with 1 au exo-Earths, with a simplified imaging noise model and other simplifying assumptions. We now turn to compare our analytic model to more-detailed computational simulations of mission yield calculations and dependencies performed for the HabEx and LUVOIR-B mission concept studies in §7.1. Both mission concepts were studied by NASA as input to the Decadal Survey on Astronomy and Astrophysics 2020 (NAP 2023), which recommended the development of a science and technology maturation program leading to the Habitable Worlds Observatory future direct imaging mission of comparable scale to these two mission concepts. These detailed HabEx and LUVOIR simulations included more complex noise models, target lists and other treatments, and herein we aim to see if these treatments are consistent with our simplified analytic model, and vice-versa. We then compare our analytic scaling dependencies to the analytical treatment in Agol (2007), and those derived from more detailed computational simulations in Stark et al. (2014), in §7.2 and §7.3 respectively. Finally, we discuss how key mission parameter choices impact Exo-Earth yield, which will be useful in future mission design trade studies to supplement more detailed computational simulations in §7.4.

7.1. Applications to HabEx & LUVOIR-B

In Table 1, we list assumed and calculated model parameter values common to both our HabEx and LUVOIR models, and values specific to either HabEx or LUVOIR, such as the telescope diameter, in Tables 2 and 3 respectively. Most values are adopted directly from assumed values either the HabEx and/or LUVOIR reports (Team 2019; Gaudi et al. 2020), and the Standards and Definitions Team report (Morgan et al. 2019). For our simplified SNR noise model, we calculate r' through a fixed-origin linear regression fit between C_{p0} and C_b on the EXOSIMS data found in Table 7 of Morgan et al. (2019) for the 9 target stars simulated. This resulted in a value of $r' = 8.75 \pm 2.29$. with an $r^2 = 0.64$ goodness of fit statistic. With the exception of HIP 17651, our model predicts the EXOSIMS exposure time estimates for the remaining 8 targets to $98 \pm 19\%$. In other words, our simple SNR photon and background noise model for estimating target exposures times is a reasonable approximation to within $\sim 20\%$ of the more detailed calculations carried out in EXOSIMS. By comparison, the Altruistic Yield Optimization tool (AYO) estimates exposure times with an average fractional difference of 56% compared to the estimated EXOSIMS exposure times (Table 7, Morgan et al. 2019). Given that these two more detailed computational simulations predict exposure times that differ on average by 56%, and our toy noise model that predicts the EXOSIMS times to within

Table 1. General values

Variable	Value	Units	Provenance
ρ_*	0.05	pc ⁻³	CH, MJ
a	1	au	IAU
η_{\oplus}	0.24	...	SDET
λ	500	nm	this work
r'	8.75	...	this work
r	9.75	...	this work
r_*	$6.957 \cdot 10^8$	m	IAU
t_*	5772	K	IAU
ε	0.5	...	G20
$\lambda/\Delta\lambda$	140	...	G20, L19
R	$1.81218 \cdot 10^{43}$	s ⁻¹	Eqn 65
K	$1 \cdot 10^{-10}$...	G20, L19

NOTE— r_* and t_* are the radius and temperature of a solar analogue.

References—SDET: [Morgan et al. \(2019\)](#), CH: [Chabrier \(2001\)](#), IAU: [Mamajek et al. \(2015\)](#), MJ: [Mamajek \(2019\)](#), G20: [Gaudi et al. \(2020\)](#), L19: [Team \(2019\)](#)

20%, our model is thus a reasonable and adequate approximation for our purposes.

Next, R was calculated from Planck's law for each survey:

$$R(\nu) = B_{\nu}(\nu, T_*) \cdot \frac{1}{h\nu} \cdot 4\pi r_*^2 \cdot 4\pi \cdot \nu \cdot \frac{\Delta\lambda}{\lambda} \quad (65)$$

$$= \frac{32\pi^2 r_*^2 c \Delta\lambda}{\lambda^4 \left(e^{\frac{hc}{\lambda k T_*}} - 1 \right)} \quad (66)$$

Finally, we assume a stellar density of 0.05 Sun-like stars per cubic parsec, which is approximately the stellar mass density of main sequence stars in the Solar Neighborhood excluding mid and late M dwarfs, given that we assume solely Sun-like stars in this work ([Chabrier 2001](#); [Mamajek 2019](#)).

In Figure 1 we plot the expected Exo-Earth yield as a function of telescope diameter for HabEx and LUVOIR compared to our model. First, we find that our LUVOIR yield model is in agreement with the more detailed computational simulation yield in [Team \(2019\)](#), whereas the estimated yield for HabEx is $\sim 50\%$ lower than our model predicts [Gaudi et al. \(2020\)](#). Specifically, the HabEx yield estimate of 8

Table 2. HabEx-specific values

Variable	Value	Units	Provenance
SNR_0	7	...	G20
N_{\oplus}	8	...	G20
d	4	m	G20
T	$0.55 \cdot 2$	yr	G20
n_i	3	...	G20

NOTE— T was calculated by multiplying the survey duration (two years) by a percent time efficiency (55%), resulting in an estimate of the total on-sky time. R was calculated as described above.

References—G20: [Gaudi et al. \(2020\)](#)

Exo-Earths is indicated with a green dot compares to our estimates of 16 and 15 for the precursor and no precursor knowledge cases at the same telescope diameter. For the LUVOIR yield estimate of 28 Exo-Earths, our model predicts yields of 30 and 30 for the precursor and no precursor knowledge cases at the same telescope diameter, a difference of $<10\%$. Second, we find that there is no benefit in the Exo-Earth yield from precursor knowledge at this telescope diameter range; of course this ignores additional benefits such as providing contemporaneous mass measurements or orbit determination, and the benefit in survey efficiency which we discuss below. The benefit of precursor knowledge for Exo-Earth yield is limited to diameters $\gtrsim 10$ -m for these assumed mission parameter values.

In Figure 2, we plot the expected Exo-Earth yield as a function of inner-working angle for HabEx and LUVOIR compared to our model. Here we see that there is no benefit from precursor knowledge as a function of inner working angle for the mission parameters and assumed iwa . However, if smaller iwa becomes technically feasible in the future – e.g. an $iwa = 2$ – then there can be a significant (factor of ~ 2) yield boost from precursor knowledge.

Next, in Figure 3, we plot the Exo-Earth yield as a function of survey duration for HabEx and LUVOIR compared to our model. First, we see for the model, the (perfect) precursor knowledge provides a substantial factor of a several reduction in survey time needed to reach the same Exo-Earth yield. At a yield of 10 Exo-Earths, for HabEx this corresponds to a reduction in on-sky time from 37.37 to 4.42 days (a factor of ~ 8.5), and for LUVOIR a reduction from 4.65 to 0.8 days (a factor of ~ 5.7). Note our simulations assume a single visit per target, which can be scaled for multiple visits. For both HabEx and LUVOIR and their expected yields, we see the estimated survey duration is longer than our estimated

Table 3. LUVOIR-specific values

Variable	Value	Units	Provenance
SNR_0	5	...	L19
N_{\oplus}	28	...	L19
d	6.7	m	L19
T	$0.55 \cdot 2$	yr	L19
n_i	4	...	L19

NOTE—As before, T was calculated by multiplying the survey duration (two years) by a percent time efficiency (55%). R was calculated as described above.

References—L19: Team (2019)

survey time for a single visit with no precursor knowledge (three times longer in the case of LUVOIR). This is consistent with needing to account for multiple visits per star. Note in all cases, we also do not account for slews and target acquisition times in calculating on-sky survey duration, which is captured in more detailed computational simulations.

7.2. Comparison to Agol (2007)

The assumptions presented in Agol (2007) are most closely analogous to those of the photon-noise-limited case without precursor knowledge. Agol (2007) finds that $N_{\oplus} \propto T^{1/3}$ when limited by PSF noise. This paper finds a higher proportionality when the inner working angle requirement is not considered: $N_{\oplus} \propto T^{3/5}$. The proportionality is less clear when we include the inner working angle requirement: by reparameterizing equation 47 with $x = N_*^{2/3}$, we can see that it is a quintic. There is no general formula for the roots of a quintic. We can see from equation 46 that the result will be weaker than $T^{3/5}$ for $\beta > 0$ ($\beta = 0$ represents a lack of the inner working angle requirement, and gives the 3/5 power), but it won't be a simple power law.

Agol (2007) also finds that $N_{\oplus} \propto SNR_0^{-1}$. We find a similar exponent when the inner working angle requirement is not considered: $N_{\oplus} \propto SNR_0^{-6/5}$. The proportionality is less clear when we include the inner working angle requirement, but it will again be weaker than $SNR_0^{-6/5}$ for $\beta > 0$, as can be seen from equation 46.

We attribute some of the differences between our results and those presented in Agol (2007) to the differences in the assumptions that were made. Specifically, assumptions about stellar spectral type, observation wavelength, semi-major axis, and noise sources differed between our models.

Regarding the first assumption, Agol (2007) took into account variable spectral types using the local interstellar mass function, whereas we assumed Solar type stars; we defer to a future work investigating for our models the impact on Exo-Earth yield with stellar mass / spectral type.

7.3. Comparison to Stark et al. (2014)

As mentioned in the captions for Figures 1, 2, and 3, there are analogous figures in Stark et al. (2014) and power-law fits to more detailed computational simulations. For the dependence of Exo-Earth yield on telescope diameter, Stark et al. (2014) finds a dependence of $N_{\oplus} \propto d^{1.8}$. For our model, Equation 43 applies in the photon-noise limited regime with no precursor knowledge:

$$d = \frac{n}{\sqrt{2}} \sqrt[3]{\frac{3N_{\oplus}}{4\pi\rho_*\eta_{\oplus}}} \sqrt{1 + \sqrt{1 + \frac{9216r^2SNR_0^4N_{\oplus}^2}{25R^2K^2\varepsilon^2n^4T^2\eta_{\oplus}^2}}} \quad (43)$$

This is not a simple power-law that can be inverted for N_{\oplus} , but we can take two simple limits to establish some bounding cases. First, in the limit that $\frac{9216r^2SNR_0^4N_{\oplus}^2}{25R^2K^2\varepsilon^2n^4T^2\eta_{\oplus}^2} \gg 1$, we have that:

$$N_{\oplus} = \eta_{\oplus} \sqrt[5]{\frac{125d^6\pi^2\rho_*^2R^3K^3T^3\varepsilon^3}{62208SNR_0^6r^3}} \quad (14)$$

and we find a shallower dependence on telescope diameter $N_{\oplus} \propto d^{6/5}$ than in Stark et al. (2014). However, Stark et al. (2014) does take into account multiple visits, which is in some sense taking into account the impact of iwa and precursor knowledge. In our model, a second bounding case can be established by the minimum telescope diameter in the iwa limited regime, which is equivalent to Equation 43 in the limit of $\frac{9216r^2SNR_0^4N_{\oplus}^2}{25R^2K^2\varepsilon^2n^4T^2\eta_{\oplus}^2} \ll 1$:

$$d = \frac{n_i\lambda}{a} \sqrt[3]{\frac{3N_{\oplus}}{4\pi\rho_*\eta_{\oplus}}} \quad (54)$$

which solving for N_{\oplus} yields Equation 59 with an equality rather than the limit:

$$N_{\oplus} = \frac{4\pi\rho_*\eta_{\oplus}a^3d^3}{3n_i^3\lambda^3} \quad (67)$$

or a dependence on telescope diameter of $N_{\oplus} \propto d^3$. Thus the Stark et al. (2014) power-law fit lies between these two bounding cases established by our model.

Next, Figure 8 in Stark et al. (2014) also evaluates the Exo-Earth yield as a function of iwa and finds a dependence of $N_{\oplus} = 100.95 - 78.44 \times iwa^{0.13}$. We find a qualitatively similar curve in Figure 2, but a different functional form. From Equation 43, we assumed $iwa = n_i\lambda/d$, which is encapsulated in our variable $n \equiv n_i\lambda/a$. To re-express 43 in terms of iwa ,

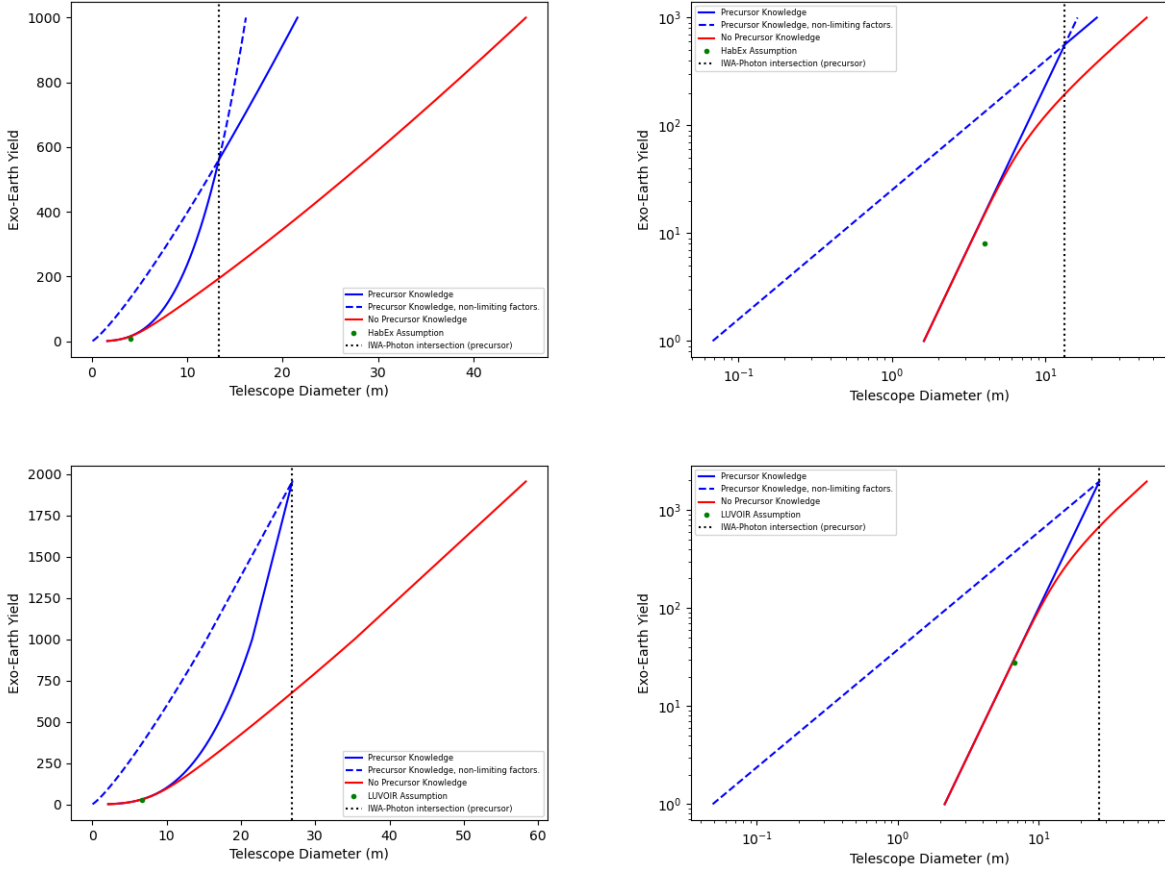


Figure 1. The number of Exo-Earth candidates detected as a function of telescope diameter with and without precursor knowledge, comparable to the upper left of Fig. 8 (linear) and 11 (logarithmic) in Stark et al. (2014), shown for HabEx with linear (top-left) and logarithmic axes (top-right), and for LUVOIR with linear (bottom-left) and logarithmic (bottom-right) axes. While the two model curves may look identical, there are differing assumptions for HabEx and LUVOIR mission parameters as detailed in Tables 2 and 3.

$iwa = na/d$, and canceling a factor of d from both sides, we have:

$$1 = \frac{iwa}{a\sqrt{2}} \sqrt[3]{\frac{3N_{\oplus}}{4\pi\rho_*\eta_{\oplus}}} \sqrt{1 + \sqrt{1 + \frac{9216r^2SNR_0^4N_{\oplus}^2a^4}{25R^2K^2\varepsilon^2iwa^4d^4T^2\eta_{\oplus}^2}}} \quad (68)$$

This is a non-trivial equation for $N_{\oplus}(iwa)$, but we can consider two limiting case power laws as we did previously. First, in the limit that $\frac{9216r^2SNR_0^4N_{\oplus}^2a^4}{25R^2K^2\varepsilon^2iwa^4d^4T^2\eta_{\oplus}^2} \gg 1$, we have that N_{\oplus} is independent of iwa , which corresponds to the photon-noise limited regime as one would expect:

$$N_{\oplus} = \eta_{\oplus} \sqrt[5]{\frac{125\pi^2\rho_*^3R^3K^3\varepsilon^3T^3d^6}{62208r^3SNR_0^6}} \quad (69)$$

Second, in the limit $\frac{9216r^2SNR_0^4N_{\oplus}^2a^4}{25R^2K^2\varepsilon^2iwa^4d^4T^2\eta_{\oplus}^2} \ll 1$, we have in the inner working angle limited regime with no precursor knowl-

edge:

$$N_{\oplus} = \frac{\eta_{\oplus}4\pi\rho_*a^3}{3iwa^3} \quad (70)$$

This is quite a large range from our two limiting scenarios, and thus depending on the mission parameter choices, the Exo-Earth yield can range from very little to a very steep dependence on the mission iwa . To support this conclusion, we note Figure 8 in Stark et al. (2015) (not to be confused with the similar Figure 8 in Stark et al. (2014)) evaluates a dependence of $iwa^{-0.98}$ for that assumed mission architecture, whereas the dependence on iwa in Gaudi et al. (2020) is relatively flat.

Finally, in Figure 10, Stark et al. (2014) investigates the survey Exo-Earth yield as a function of total on-sky time, the reciprocal of our Figure 3, and finds that the yield scales as mission duration $T^{0.41}$. Again, from Equation 43, we can solve for T as a function of N_{\oplus} , but not in the inverse. For the latter we must use the same two prior approximations:

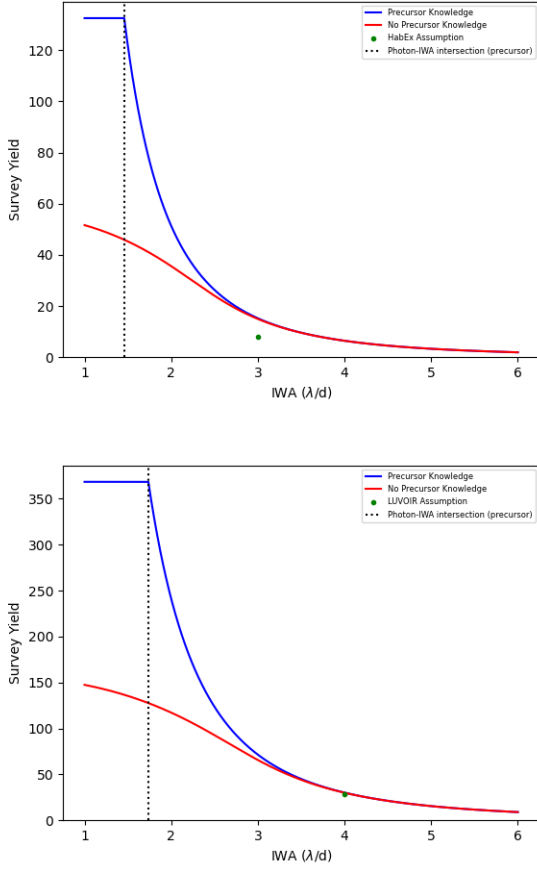


Figure 2. The number of ExoEarth Candidates detected vs telescope iwa with and without precursor knowledge, comparable to the upper right of Fig. 8 in Stark et al. (2014), for HabEx (top) and LUVOIR (bottom).

$$T = \frac{48 \times 3^{\frac{2}{3}} SNR^2 N_{\oplus}^{\frac{5}{3}}}{5RK\epsilon d(4\pi\rho_*)^{\frac{1}{3}} \eta_{\oplus}^{\frac{4}{3}} \sqrt{d^2(4\pi\rho_*\eta_{\oplus})^{\frac{2}{3}} - n^2(3N_{\oplus})^{\frac{2}{3}}}} \quad (71)$$

In the limit that $\frac{9216r^2 SNR_0^4 N_{\oplus}^2}{25R^2 K^2 \epsilon^2 n^4 T^2 \eta_{\oplus}^2} \gg 1$, which can be thought of the short survey duration limited case, we again derive:

$$N_{\oplus} = \eta_{\oplus} \sqrt[5]{\frac{125d^6 \pi^2 \rho_*^2 R^3 K^3 T^3 \epsilon^3}{62208 SNR_0^6 r^3}} \quad (14)$$

and in the limit of $\frac{9216r^2 SNR_0^4 N_{\oplus}^2}{25R^2 K^2 \epsilon^2 n^4 T^2 \eta_{\oplus}^2} \ll 1$, which can be thought of as the long survey duration case, we again derive:

$$N_{\oplus} = \frac{4\pi\rho_*\eta_{\oplus}a^3 d^3}{3n^3 \lambda^3} \quad (67)$$

In other words, for long-enough survey durations, you run out of targets to image and the survey yield asymptotes to be

independent of survey duration; this is the vertical asymptote in Figure 3. Specifically then, we find that $N_{\oplus} \propto T^{3/5}$ in the short survey duration regime, slightly steeper than the power law in Stark et al. (2014), although without the zero point offset.

7.4. Evaluating the Dependence of Exo-Earth Yield on Mission Parameter Choices, Trades, and Precursor Knowledge

In the previous section, we evaluated the dependence of Exo-Earth yield on the telescope diameter d , the iwa and on sky survey duration T in the absence of precursor knowledge, which is given by Equation 43 in a simplifying limit when we are inner working angle limited and goes as Equation 14:

$$d = \frac{n}{\sqrt{2}} \sqrt[3]{\frac{3N_{\oplus}}{4\pi\rho_*\eta_{\oplus}}} \sqrt{1 + \sqrt{1 + \frac{9216r^2 SNR_0^4 N_{\oplus}^2}{25R^2 K^2 \epsilon^2 n^4 T^2 \eta_{\oplus}^2}}} \quad (43)$$

$$N_{\oplus} = \eta_{\oplus} \sqrt[5]{\frac{125d^6 \pi^2 \rho_*^2 R^3 K^3 T^3 \epsilon^3}{62208 SNR_0^6 r^3}} \quad (14)$$

In the case of precursor knowledge, there is a gain in yield derived in both the scenarios considered in equations 27 and 50:

$$N_{\oplus} = \sqrt[5]{\frac{125\pi^2 d^6 R^3 K^3 T^3 \epsilon^3 \rho_*^2 \eta_{\oplus}^2}{62208 r^3 SNR_0^6}} \quad (27)$$

$$N_{\oplus} = \sqrt[5]{\frac{125\pi^2 d^6 R^3 K^3 T^3 \epsilon^3 \rho_*^2 \eta_{\oplus}^2}{62208 r^3 SNR_0^6}} \quad (50)$$

All of the factors are identical to the no precursor knowledge case with one exception: the Exo-Earth yield for the precursor knowledge cases have a missing factor of η_{\oplus} , which is < 1 and is thus a gain to N_{\oplus} . This yield gain can be thought of as a direct consequence of surveying only N_{\oplus} stars instead of $N_{\oplus}\eta_{\oplus} = N_*$ stars as is the case with no precursor knowledge, and is thus primarily realized through enabling a shorter survey duration in the inner working angle limited regime represented by Equations 14, 27, and 50.

While we find that, as intuitively expected, the Exo-Earth yield of a mission with no precursor knowledge scaled with η_{\oplus} , as also captured as an approximately linear relation in Figure 14 of Stark et al. (2015), this is not the case for a survey with precursor knowledge as seen in Equations 50 and 27. In the case of precursor knowledge, the dependence on η_{\oplus} is a much shallower power law of $\frac{2}{5}$. In other words, precursor knowledge, such as might be obtained by ground-based precise radial velocities or astrometry, reduces the sensitivity and thus the risk of the yield of a future direct imaging mission to our current knowledge of η_{\oplus} and its uncertainty (e.g., Bryson et al. 2021; Zink et al. 2019, and references therein).

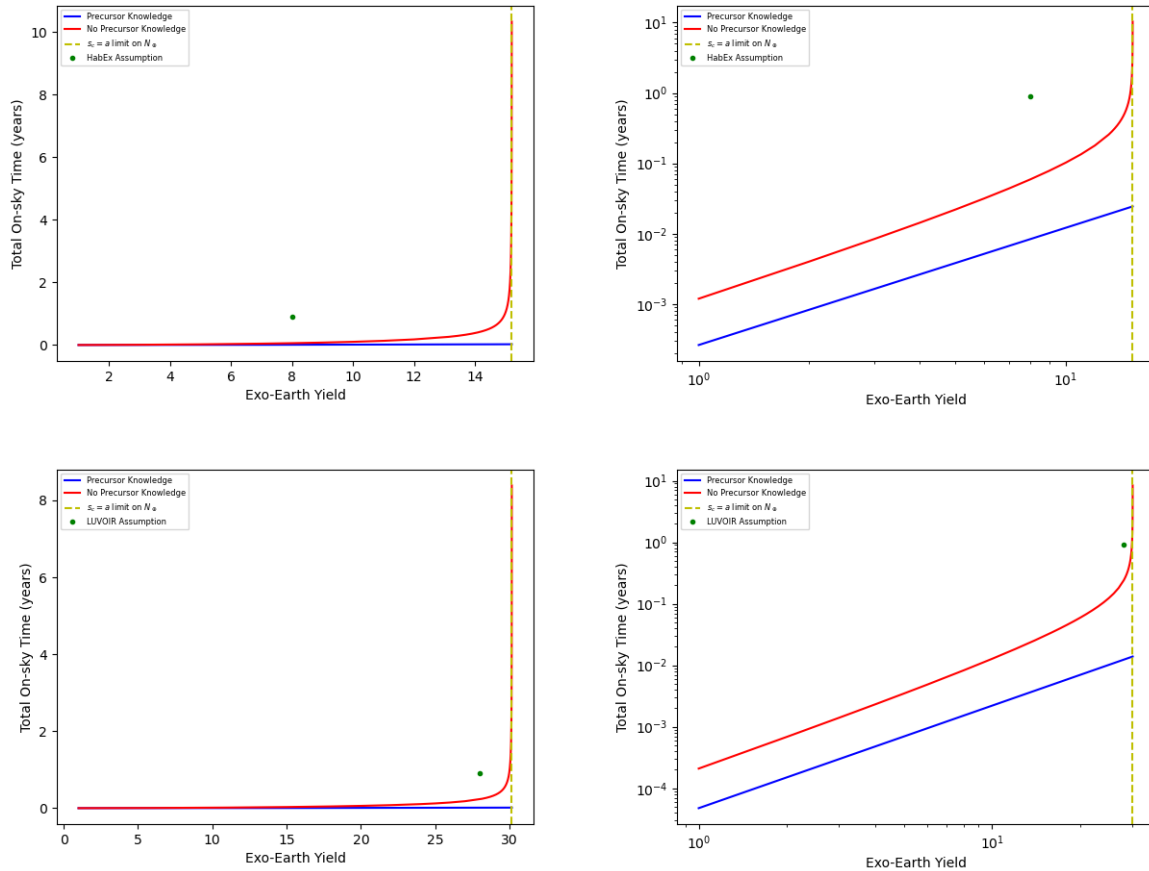


Figure 3. The necessary total on-sky time as a function of required survey yield, with and without precursor knowledge. Note that we gain significant time-efficiency improvements from precursor knowledge as we approach the IWA-mandated yield limit. The top panels are for HabEx, and the bottom for LUVOIR. The left panels are for a linear vertical axis, and logarithmic for the right panels. This figure is a flipped-axis version of Fig. 10 in Stark et al. (2014). Note, our survey durations do not include multiple revisits, slew and overhead times, explaining our significantly shorter survey durations.

Next, throughout this work we have assumed “perfect” precursor knowledge, when astrometry and radial velocities in general will provide incomplete knowledge of exoplanet systems, either from the lack of a known inclination for radial velocities, or limits to exoplanet mass sensitivity for both techniques that are currently both well above the Earth-mass regime. So the actual impact of precursor knowledge will lie somewhere between our two limiting scenarios of whether or not precursor knowledge is available for a future direct imaging mission. We have now quantified that benefit analytically as presented herein in terms of Exo-Earth yield and survey efficiency, in support of community evaluations of EPRV precursor surveys in Crass et al. (2021) and the numerical simulations in Morgan et al. (2021). Even without “perfect” precursor knowledge, more massive planets discovered with precursor radial velocities located in the HZ of target stars can dynamically preclude the presence of HZ Exo-Earths in a given system (Hill et al. 2018; Kane & Blunt 2019; Kane et al. 2020), which can in turn help optimize target selec-

tion, HZ exo-moons aside (Kipping et al. 2022; Teachey et al. 2018). In addition to mass sensitivity, there is also a need for ephemerides refinement of known more massive planets in the systems of interest discovered with the radial velocity technique, regardless of orbital semi-major axis, to more accurately forecast orbital phase at the imaging epochs to aid in planet identification for what will hopefully be bountiful multi-planet systems when imaged (e.g., “which is which,” Kane et al. 2009).

Finally, while we have shown how the Exo-Earth yield scales with iwa , telescope diameter d , survey duration T , η_{\oplus} , the same can also be done for SNR_0 , flux contrast K , spectral resolution R , approximate noise model enhancement factor r , planet semi-major axis a , target stellar density ρ_* , and telescope throughput efficiency ϵ by differentiating equations presented herein, or through point comparison deltas. This can potentially be very useful in quick “rules-of-thumb” in the coming decade’s trade studies in mission and telescope design, and instrument parameters.

8. CONCLUSIONS

We have calculated simple analytic expressions for the yield of a future flagship direct imaging mission such as Habitable Worlds Observatory as a function of various key mission design parameters under the assumption of identical and uniformly distributed Sun-like stars. We find that the HabEx and LUVOIR mission concept yield simulations of Earth-like planets are consistent with our analytic model, with little increase in yield from precursor knowledge. However, the benefit from precursor knowledge can increase greatly for larger-yield or larger telescope diameter surveys, or for surveys that require higher SNR and spectral resolution than base-lined for the HabEx and LUVOIR mission concepts. Additionally, we find that precursor knowledge reduces the mission risk (sensitivity) to our Exo-Earth yield given our current knowledge of η_{\oplus} and its uncertainty. Next, we find that the survey efficiency is greatly enhanced by precursor knowledge such as can be provided by extremely precise radial velocities and astrometry, consistent with precursor detailed computational simulations. We also find qualitatively similar agreement to HabEx and LUVOIR yield estimates, and for the dependence of yield of several key mission parameters from more detailed computational simulations. These consistent results provide an analytic check on these more detailed simulations. We have provided a set of relations that allow for fast estimates of the analytic dependence of Exo-Earth yield on key mission, telescope and instrument parameters, both in the bounding cases of no precursor knowledge and full precursor knowledge. In the future, we could explore modifying our analytical model to include a range of spectral types and semi-major axes, as well as for a range of different planet populations.

ACKNOWLEDGEMENTS

PPP and JEB contributed equally to this work. As a high school research intern from 2019-2022, JEB derived most of the analytic relations under the analytic framework and mentorship provided by PPP. JEB developed all of the software for generating figures. PPP performed most of the writing and organization. SE provided initial investigations in a prior year as a summer research intern. SRK, RM and EP provided detailed feedback and expert guidance to the development of the research.

We thank Karl Stapelfeldt, Eric Mamajek, Scott Gaudi, Thayne Currie, Bryson Cale, and Chris Stark for useful conversations leading to motivating this research and feedback on this analysis over nearly a decade from its initial concept formulation at the start of the HabEx mission concept study. PPP was a member of and acknowledges support from the HabEx STDT and the Standards and Definitions Team.

JEB would like to acknowledge Dr. John E. Berberian, Sr., for the derivation of the better approximation for the finite

power-law summation relative to the integral limit.

PPP would like to acknowledge support from NASA (Exoplanet Research Program Award #80NSSC20K0251, TESS Cycle 3 Guest Investigator Program Award #80NSSC21K0349, JPL Research and Technology Development, and Keck Observatory Data Analysis) and the NSF (Astronomy and Astrophysics Grants #1716202 and 2006517), and the Mt Cuba Astronomical Foundation.

9. APPENDIX A

9.1. Derivation of η_{\oplus} dependence of $\sum_{k=1}^{N_*} k^{2/3}$.

Because of the properties of telescoping series, we know that:

$$\begin{aligned} (N_* + 1)^{p+1} - 1 &= \sum_{k=1}^{N_*} (k+1)^{p+1} - k^{p+1} \\ &= \sum_{k=1}^{N_*} k^{p+1} \left(\left(1 + \frac{1}{k}\right)^{p+1} - 1 \right) \end{aligned}$$

Using a binomial series expansion, we get:

$$\begin{aligned} (N_* + 1)^{p+1} - 1 &= \sum_{k=1}^{N_*} k^{p+1} \left(-1 + \sum_{\ell=0}^{\infty} \binom{p+1}{\ell} k^{-\ell} \right) \\ &= \sum_{k=1}^{N_*} k^{p+1} \sum_{\ell=1}^{\infty} \binom{p+1}{\ell} k^{-\ell} \\ &= \sum_{k=1}^{N_*} \sum_{\ell=1}^{\infty} \binom{p+1}{\ell} k^{p+1-\ell} \\ &= \sum_{\ell=1}^{\infty} \binom{p+1}{\ell} \sum_{k=1}^{N_*} k^{p+1-\ell} \end{aligned}$$

We now define S_n such that

$$S_n = \sum_{k=1}^{N_*} k^n.$$

Thus,

$$\begin{aligned} (N_* + 1)^{p+1} - 1 &= \sum_{\ell=1}^{\infty} \binom{p+1}{\ell} S_{p+1-\ell} \\ (N_* + 1)^p - 1 &= \sum_{\ell=1}^{\infty} \binom{p}{\ell} S_{p-\ell} \\ (N_* + 1)^{p-1} - 1 &= \sum_{\ell=1}^{\infty} \binom{p-1}{\ell} S_{p-1} \\ &\cdot \\ &\cdot \\ &\cdot \end{aligned}$$

A useful representation of this equality is the multiplication of a matrix with a vector.

$$\begin{bmatrix} (N_* + 1)^{p+1} - 1 \\ (N_* + 1)^p - 1 \\ (N_* + 1)^{p-1} - 1 \\ \cdot \\ \cdot \\ \cdot \end{bmatrix} = \begin{bmatrix} \binom{p+1}{1} & \binom{p+1}{2} & \binom{p+1}{3} & \cdot & \cdot \\ 0 & \binom{p}{1} & \binom{p}{2} & & \\ 0 & 0 & \binom{p-1}{1} & & \\ \cdot & & & & \\ \cdot & & & & \\ \cdot & & & & \end{bmatrix} \begin{bmatrix} S_p \\ S_{p-1} \\ S_{p-2} \\ \cdot \\ \cdot \\ \cdot \end{bmatrix}$$

We now assume that a 2x2 matrix is sufficient to approximate this within acceptable error. We will verify this assumption for $p = \frac{2}{3}$ later.

$$\begin{bmatrix} (N_* + 1)^{p+1} - 1 \\ (N_* + 1)^p - 1 \end{bmatrix} \approx \begin{bmatrix} \binom{p+1}{1} & \binom{p+1}{2} \\ 0 & \binom{p}{1} \end{bmatrix} \begin{bmatrix} S_p \\ S_{p-1} \end{bmatrix}$$

We now apply Cramer's rule to solve for S_p :

$$S_p = \frac{\begin{vmatrix} (N_* + 1)^{p+1} - 1 & \binom{p+1}{2} \\ (N_* + 1)^p - 1 & \binom{p}{1} \end{vmatrix}}{\begin{vmatrix} \binom{p+1}{1} & \binom{p+1}{2} \\ 0 & \binom{p}{1} \end{vmatrix}}$$

$$= \frac{p \left((N_* + 1)^{p+1} - 1 \right) - \frac{p(p+1)}{2} \left((N_* + 1)^p - 1 \right)}{p(p+1)}$$

$$= \frac{(N_* + 1)^{p+1}}{p+1} - \frac{(N_* + 1)^p}{2} + \left(\frac{1}{2} - \frac{1}{p+1} \right)$$

This approximation of $\sum_{k=1}^{N_*} k^p$ for $p = \frac{2}{3}$ has an error of 1.118074% at $N_* = 1$, and an error of 0.000083% at $N_* = 1000$, and as N_* grows, the error continues to decrease. For the purposes of this paper, this error is insignificant.

So,

$$\sum_{k=1}^{N_*} k^{2/3} \approx \frac{3(N_* + 1)^{5/3}}{5} - \frac{(N_* + 1)^{2/3}}{2} - \frac{1}{10} \quad (72)$$

10. APPENDIX B

10.1. Derivation of Time Fraction Usable

We assume that the exoplanet's orbit is circular, with some inclination i relative to the viewer. This will make one on-sky axis fore-shortened, by a uniform random factor of $1 \geq \cos i \geq 0$. From the viewer's perspective, the exoplanet traces an ellipse, described by the equations

$$x_p(t) = a \cos(t)$$

$$y_p(t) = a \sin(t) \cos i$$

Table 4. Cases for time fraction usable

Axis	Value Relative to s_c								
	<	=	>	<	=	>	<	=	>
a	<	=	>	<	=	>	<	=	>
$a \cos i$	<	<	<	=	=	=	>	>	>
Case	A	B	C	...	D	E	F

where a is the semi-major axis of the planet. Note that we arbitrarily chose to shorten the y_p dimension; because the viewer's perspective can be rotated.

We now project the inner working angle of the telescope onto that ellipse. This creates a circle of radius

$$s_c = D_k \cdot iwa. \quad (73)$$

A usable observation is one that occurs when $x_p^2 + y_p^2 > s_c^2$ holds; that is, when the exoplanet in question is outside the circle. The fraction of time usable will vary depending on the relationship between these variables. To ensure that we have explored all options, we will refer to the following case table. We do not enumerate the cases that violate the restriction that $\cos i \leq 1$.

10.1.1. Derivation of Time Fraction Usable - Case A

Both axes of the ellipse, a and $a \cos i$, are less than s_c . This means that the ellipse is completely enclosed inside the circle. We can always say that $x_p^2 + y_p^2 < s_c^2$, so we cannot make any usable observations. The usable time fraction for this case is 0.

10.1.2. Derivation of Time Fraction Usable - Case B

This time, $a = s_c$, but $a \cos i < s_c$. The ellipse is tangent to the circle at two points, but it is still completely enclosed by the circle. We can always say that $x_p^2 + y_p^2 \leq s_c^2$, so we cannot make any usable observations. The time fraction usable is 0.

10.1.3. Derivation of Time Fraction Usable - Case C

This one is the most difficult case. $a > s_c > a \cos i$, so the expression $x_p^2 + y_p^2 > s_c^2$ sometimes holds, so we only sometimes get usable observations. Fortunately, we can derive the fraction of time usable for this case.

Substituting our expression for y_p into that inequality:

$$x_p^2 + a^2 \sin^2(t) \cos^2 i > s_c^2$$

We can use a Pythagorean identity to get everything in terms of x_p :

$$x_p^2 + \cos^2 i (a^2 - a^2 \cos^2(t)) > s_c^2$$

$$x_p^2 + \cos^2 i (a^2 - x_p^2) > s_c^2$$

Solving for x_p^2 in terms of the other variables:

$$x_p^2 - x_p^2 \cos^2 i > s_c^2 - a^2 \cos^2 i$$

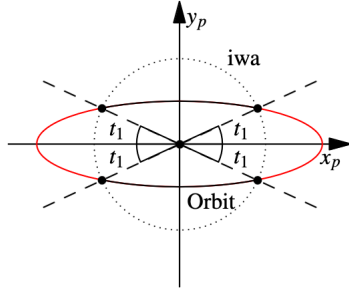


Figure 4. Example of Case C orbit, usable times are highlighted in red.

$$x_p^2 (1 - \cos^2 i) > s_c^2 - a^2 \cos^2 i$$

$$x_p^2 > \frac{s_c^2 - a^2 \cos^2 i}{1 - \cos^2 i}$$

To ensure that the last step - dividing by $1 - \cos^2 i$ - was valid, we can examine the available values for $\cos^2 i$. Recall that in this case, $a > s_c > a \cos i$. If $\cos i = 1$, then $a = a \cos i$, which violates the base assumption for this case. So, $\cos i < 1$, and $1 - \cos^2 i > 0$. Moving on, we can take the square root of both sides:

$$x_p > \sqrt{\frac{s_c^2 - a^2 \cos^2 i}{1 - \cos^2 i}}$$

OR

$$x_p < -\sqrt{\frac{s_c^2 - a^2 \cos^2 i}{1 - \cos^2 i}}$$

At the intersections,

$$x_p = \pm \sqrt{\frac{s_c^2 - a^2 \cos^2 i}{1 - \cos^2 i}}$$

These are the x-values for the intersections, but it would be useful to get y-values too.

$$y_p^2 = a^2 \cos^2(t) \cos^2 i$$

$$= \cos^2 i (a^2 - a^2 \sin^2(t))$$

$$= \cos^2 i (a^2 - x^2)$$

Again, taking the square root,

$$y_p = \pm \cos i \sqrt{a^2 - \frac{s_c^2 - a^2 \cos^2 i}{1 - \cos^2 i}}$$

Notably, both the x_p and y_p have \pm symmetry. An example of this is shown below, with the usable times highlighted in red.

Because of the symmetry, all the angles will be the same. We will call that angle measure t_1 . We can easily find t_1 from the x_p value at one of the intersections. For simplicity's sake, we will choose the positive x_p intersection value.

$$x_p = a \cos(t_1) = \sqrt{\frac{s_c^2 - a^2 \cos^2 i}{1 - \cos^2 i}}$$

$$\cos(t_1) = \frac{1}{a} \sqrt{\frac{s_c^2 - a^2 \cos^2 i}{1 - \cos^2 i}}$$

$$t_1 = \cos^{-1} \left(\frac{1}{a} \sqrt{\frac{s_c^2 - a^2 \cos^2 i}{1 - \cos^2 i}} \right)$$

Where \cos^{-1} denotes the inverse cosine function. Because there are four such angles, we should multiply this by four.

$$4t_1 = 4 \cos^{-1} \left(\frac{1}{a} \sqrt{\frac{s_c^2 - a^2 \cos^2 i}{1 - \cos^2 i}} \right)$$

This gives us the total angle measure in which usable observations can be made. We want this as a fraction of the 2π , though. We will assume that the angle measure is equivalent to time. Then, the time fraction usable t_f would be:

$$t_f = \frac{4}{2\pi} \cos^{-1} \left(\frac{1}{a} \sqrt{\frac{s_c^2 - a^2 \cos^2 i}{1 - \cos^2 i}} \right)$$

$$= \frac{2}{\pi} \cos^{-1} \left(\frac{1}{a} \sqrt{\frac{s_c^2 - a^2 \cos^2 i}{1 - \cos^2 i}} \right)$$

So, the usable fraction of time for this case is

$$\frac{2}{\pi} \cos^{-1} \left(\frac{1}{a} \sqrt{\frac{s_c^2 - a^2 \cos^2 i}{1 - \cos^2 i}} \right). \quad (74)$$

10.1.4. Derivation of Time Fraction Usable - Case D

Because $a = a \cos i = s_c$, $x_p^2 + y_p^2 = s_c^2 \cos^2(t) + s_c^2 \sin^2(t)$, which is always s_c^2 . Unfortunately, $s_c^2 > s_c^2$ is never true, so we will never get usable observations for this case. The fraction of usable time is 0.

10.1.5. Derivation of Time Fraction Usable - Case E

$a > s_c = a \cos i$, so the ellipse is tangent to the circle at two points, and at all other times it is outside the circle. So, we can make usable observations on the exoplanet at all times except two. Because both those points are infinitesimally small, the fraction of time usable for this case is 1.

10.1.6. Derivation of Time Fraction Usable - Case F

Both a and $a \cos i$ are greater than s_c . This means that the inner-working-angle circle is completely enclosed inside the orbit's ellipse, so all observations will be usable. The fraction of time usable is 1.

10.2. Derivation of Average Time Fraction Usable

Because we can get no usable observations with $s_c \geq a$, we require an iwa such that $s_c < a$ for all targets.

For simplicity, it would be useful to have an average of the usable time fractions. We can achieve this by integrating the fraction of time usable across all values of $\cos i$. We can

do this without weighting because $\cos i$ is a uniform random variable.

While $0 \leq \cos i < s_c/a$, $a \cos i < s_c < a$, (Case C) so the usable time fraction is

$$\frac{2}{\pi} \cos^{-1} \left(\frac{1}{a} \sqrt{\frac{s_c^2 - a^2 \cos^2 i}{1 - \cos^2 i}} \right).$$

While $\cos i = s_c/a$, $a \cos i = s_c < a$, (Case E) so the usable time fraction is 1.

While $s_c/a < \cos i \leq 1$, $s_c < a \cos i \leq a$, (Case F) so the usable time fraction is 1.

So, our integral will be

$$\lim_{\kappa \rightarrow (\frac{s_c}{a})^-} \int_0^\kappa \frac{2}{\pi} \cdot \arccos \left(\frac{1}{a} \cdot \sqrt{\frac{s_c^2 - a^2 \cos^2 i}{1 - \cos^2 i}} \right) d(\cos i) + \int_{s_c/a}^1 1 d(\cos i)$$

Integrating 1 is trivial, but the arccosine might be harder. So, we turn to Mathematica. Evaluating the Mathematica expression

```
Limit[Integrate[2 ArcCos[Sqrt[(sc^2 - (a^2)(x^2))/(1 - x^2)]/a]/Pi, x], x->0]
```

yields

$$\frac{2\sqrt{-s_c^2} \sqrt{1 - \frac{s_c^2}{a^2}} \ln \left(a \sqrt{-s_c^2} \right)}{\sqrt{s_c^2} \pi}$$

This will be simplified in the "Lower bound" section. If we evaluate the expression

```
Limit[Integrate[2 ArcCos[Sqrt[(sc^2 - (a^2)(x^2))/(1 - x^2)]/a]/Pi, x], x -> sc/a, Direction -> "FromBelow"]
```

we get the result

$$\frac{s_c}{a} + \frac{\sqrt{-as_c}}{\pi \sqrt{\frac{a^3 s_c}{a^2 - s_c^2}} \sqrt{a^2 - s_c^2}} \left(a \ln \left(1 - \frac{s_c}{a} \right) - a \ln(s_c(a - s_c)) - a \ln \left(\frac{a + s_c}{a} \right) + 2\sqrt{a^2 - s_c^2} \ln(as_c) + a \ln(-s_c(a + s_c)) \right).$$

This will be simplified in the "Upper bound section."

10.2.1. Upper bound

Direct from Mathematica, with no simplifications:

$$\frac{s_c}{a} + \frac{\sqrt{-as_c}}{\pi \sqrt{\frac{a^3 s_c}{a^2 - s_c^2}} \sqrt{a^2 - s_c^2}} \left(a \ln \left(1 - \frac{s_c}{a} \right) - a \ln(s_c(a - s_c)) - a \ln \left(\frac{a + s_c}{a} \right) + 2\sqrt{a^2 - s_c^2} \ln(as_c) + a \ln(-s_c(a + s_c)) \right).$$

We know that $a \cos i \geq 0$, and $s_c > a \cos i$, so $s_c > 0$. Also, $a > 0$ because the planet must orbit at a nonzero distance. Thus, $ab > 0$ and $\sqrt{as_c} \neq 0$, so we can cancel it, and pull a factor of a out of the denominator's square root.

$$\frac{s_c}{a} + \frac{\sqrt{-1}}{a\pi \sqrt{\frac{1}{a^2 - s_c^2}} \sqrt{a^2 - s_c^2}} \left(a \ln \left(1 - \frac{s_c}{a} \right) - a \ln(s_c(a - s_c)) - a \ln \left(\frac{a + s_c}{a} \right) + 2\sqrt{a^2 - s_c^2} \ln(as_c) + a \ln(-s_c(a + s_c)) \right)$$

We know that $a > s_c$, so $a^2 - s_c^2 \neq 0$. So, we can cancel a $\sqrt{a^2 - s_c^2}$ in the denominator. Also, $\sqrt{-1} = i$.

$$\frac{s_c}{a} + \frac{i}{a\pi} \left(a \ln \left(1 - \frac{s_c}{a} \right) - a \ln(s_c(a - s_c)) - a \ln \left(\frac{a + s_c}{a} \right) + 2\sqrt{a^2 - s_c^2} \ln(as_c) + a \ln(-s_c(a + s_c)) \right)$$

Because the exoplanet must orbit its star at some nonzero distance, we know that $a \neq 0$. So, we can cancel a factor of a .

$$\frac{s_c}{a} + \frac{i}{\pi} \left(\ln \left(1 - \frac{s_c}{a} \right) - \ln(s_c(a - s_c)) - \ln \left(\frac{a + s_c}{a} \right) + \frac{2}{a} \sqrt{a^2 - s_c^2} \ln(as_c) + \ln(-s_c(a + s_c)) \right)$$

We can simplify the first logarithm, and cancel some factors.

$$\frac{s_c}{a} + \frac{i}{\pi} \left(\ln \left(\frac{a - s_c}{a} \right) - \ln(s_c(a - s_c)) - \ln \left(\frac{a + s_c}{a} \right) + \frac{2}{a} \sqrt{a^2 - s_c^2} \ln(as_c) + \ln(-s_c(a + s_c)) \right)$$

$$\frac{s_c}{a} + \frac{i}{\pi} \left(\ln\left(\frac{1}{a}\right) - \ln(s_c) - \ln\left(\frac{a+s_c}{a}\right) + \frac{2}{a} \sqrt{a^2 - s_c^2} \ln(as_c) + \ln(-s_c(a+s_c)) \right)$$

We can split up some of these logarithms, and turn reciprocals into minus signs.

$$\frac{s_c}{a} + \frac{i}{\pi} \left(-\ln(a) - \ln(s_c) + \frac{2}{a} \sqrt{a^2 - s_c^2} \ln(as_c) - \ln\left(\frac{a+s_c}{a}\right) + \ln(s_c) + \ln(-1) + \ln(a+s_c) \right)$$

We can cancel the $\pm \ln(s_c)$ pair, and split up the logarithms further.

$$\frac{s_c}{a} + \frac{i}{\pi} \left(-\ln(a) + \frac{2}{a} \sqrt{a^2 - s_c^2} \ln(as_c) - \ln(a+s_c) + \ln(a) + \ln(-1) + \ln(a+s_c) \right)$$

We can also cancel the $\pm \ln(a)$ and $\pm \ln(a+s_c)$ pairs.

$$\frac{s_c}{a} + \frac{i}{\pi} \left(\frac{2}{a} \sqrt{a^2 - s_c^2} \ln(as_c) + \ln(-1) \right)$$

The $\ln(-1)$ can be simplified to πi . This can easily be derived from the equation $e^{i\pi} = -1$.

$$\frac{s_c}{a} + \frac{i}{\pi} \left(\frac{2}{a} \sqrt{a^2 - s_c^2} \ln(as_c) + \pi i \right)$$

Distributing through the i/π :

$$\frac{s_c}{a} + \frac{2i}{a\pi} \sqrt{a^2 - s_c^2} \ln(as_c) - 1$$

The real and imaginary parts are now separate. We know this because a and s_c are real, and $a > s_c$, so $\sqrt{a^2 - s_c^2}$ is real. Also, we showed earlier that $ab > 0$, so $\ln(as_c)$ must also be real. Therefore, the second term is completely imaginary,

and the first term is completely real.

$$\frac{s_c - a}{a} + \frac{2i}{a\pi} \sqrt{a^2 - s_c^2} \ln(as_c)$$

10.2.2. Lower bound

Again, this is directly from Mathematica.

$$\frac{2\sqrt{-s_c^2} \sqrt{1 - \frac{s_c^2}{a^2}} \ln\left(a\sqrt{-s_c^2}\right)}{\sqrt{s_c^2} \pi}$$

We know that $s_c > 0$, so $\sqrt{s_c^2} \neq 0$, so we can cancel a factor of $\sqrt{s_c^2}$.

$$\frac{2\sqrt{-1} \sqrt{1 - \frac{s_c^2}{a^2}} \ln\left(a\sqrt{-s_c^2}\right)}{\pi}$$

We can pull a factor of a^{-1} out of the square root. Also, $\sqrt{-1} = i$

$$\frac{2i\sqrt{a^2 - s_c^2} \ln\left(a\sqrt{-s_c^2}\right)}{a\pi}$$

That logarithm can be pulled apart, and we can simplify $\sqrt{-s_c^2}$ to $s_c i$.

$$\frac{2i\sqrt{a^2 - s_c^2} (\ln(a) + \ln(s_c i))}{a\pi}$$

The logarithm can be pulled apart further.

$$\frac{2i\sqrt{a^2 - s_c^2} (\ln(a) + \ln(s_c) + \ln(i))}{a\pi}$$

We can recombine some logarithms, and the $\ln(i)$ can be simplified to $\pi i/2$. This can easily be derived from the equation $e^{i\pi/2} = i$.

$$\frac{2i\sqrt{a^2 - s_c^2} (\ln(as_c) + \frac{\pi i}{2})}{a\pi}$$

Distributing across the sum:

$$\frac{2i}{a\pi} \sqrt{a^2 - s_c^2} \ln(as_c) + \frac{2i}{a\pi} \sqrt{a^2 - s_c^2} \frac{\pi i}{2}$$

We can cancel some factors on the right.

$$\frac{2i}{a\pi} \sqrt{a^2 - s_c^2} \ln(as_c) - \frac{\sqrt{a^2 - s_c^2}}{a}$$

We have again separated the real and imaginary parts of this equation. The right is the same as last time, so we know that it is completely imaginary. The left must be real, because $\sqrt{a^2 - s_c^2}$ is real, and a is real.

$$-\frac{\sqrt{a^2 - s_c^2}}{a} + \frac{2i}{a\pi} \sqrt{a^2 - s_c^2} \ln(as_c)$$

10.2.3. Difference of bounds

Subtraction should yield the definite integral, evaluated on $0 \leq \cos i < b/a$

$$\frac{s_c - a}{a} + \frac{2i}{a\pi} \sqrt{a^2 - s_c^2} \ln(as_c) - \left(-\frac{\sqrt{a^2 - s_c^2}}{a} + \frac{2i}{a\pi} \sqrt{a^2 - s_c^2} \ln(as_c) \right)$$

Conveniently, the imaginary parts cancel cleanly, leaving only the real parts.

$$\frac{s_c - a}{a} - \left(-\frac{\sqrt{a^2 - s_c^2}}{a} \right)$$

The difference of the real parts turns out to be rather simple:

$$\frac{s_c - a + \sqrt{a^2 - s_c^2}}{a}$$

10.2.4. With $\cos i > \frac{s_c}{a}$ added in

We must also remember to integrate from $s_c/a \leq \cos i \leq 1$. However, the time fraction usable here is just 1, which makes for easy integration.

$$\int_{s_c/a}^1 1 d(\cos i) = 1 - \frac{s_c}{a}$$

Adding that in with the other part of the integral:

$$\frac{s_c - a + \sqrt{a^2 - s_c^2}}{a} + 1 - \frac{s_c}{a} = \frac{\sqrt{a^2 - s_c^2}}{a}$$

This gives us a simple, compact result.

$$\lim_{\kappa \rightarrow (\frac{s_c}{a})^-} \int_0^\kappa \frac{2}{\pi} \cdot \arccos \left(\frac{1}{a} \cdot \sqrt{\frac{s_c^2 - a^2 \cos^2 i}{1 - (\cos^2 i)}} \right) d(\cos i) + \int_{s_c/a}^1 1 d(\cos i) = \boxed{\frac{\sqrt{a^2 - s_c^2}}{a}} \tag{75}$$

11. APPENDIX C

11.1. Inversion of $\frac{m}{x^2 \sqrt{1 - (n/x)^2}}$

We need to invert the equation

$$y = \frac{m}{x^2 \sqrt{1 - (n/x)^2}}$$

We begin by squaring both sides:

$$y^2 = \frac{m^2}{x^4 \left(1 - \frac{n^2}{x^2}\right)} = \frac{m^2}{x^2 (x^2 - n^2)}$$

We rearrange the equation:

$$y^2 = \frac{m^2}{x^2 (x^2 - n^2)} \\ x^2 (x^2 - n^2) = \frac{m^2}{y^2} \\ x^4 - n^2 x^2 - \frac{m^2}{y^2} = 0$$

We apply the quadratic formula and take the square root:

$$x^2 = \frac{1}{2} \left(n^2 \pm \sqrt{n^4 + \frac{4m^2}{y^2}} \right) \\ x = \pm \sqrt{\frac{1}{2} \left(n^2 \pm \sqrt{n^4 + \frac{4m^2}{y^2}} \right)} \tag{76}$$

REFERENCES

- 2023, Pathways to Discovery in Astronomy and Astrophysics for the 2020s (Washington, DC: The National Academies Press), doi: [10.17226/26141](https://doi.org/10.17226/26141).
<https://nap.nationalacademies.org/catalog/26141/pathways-to-discovery-in-astronomy-and-astrophysics-for-the-2020s>
- Agol, E. 2007, MNRAS, 374, 1271, doi: [10.1111/j.1365-2966.2006.11232.x](https://doi.org/10.1111/j.1365-2966.2006.11232.x)
- Akeson, R. L., Chen, X., Ciardi, D., et al. 2013, Publications of the Astronomical Society of the Pacific, 125, 989, doi: [10.1086/672273](https://doi.org/10.1086/672273)
- Bailer-Jones, C. A. L., Rybizki, J., Fouesneau, M., Mantelet, G., & Andrae, R. 2018, AJ, 156, 58, doi: [10.3847/1538-3881/aacb21](https://doi.org/10.3847/1538-3881/aacb21)
- Brown, R. A. 2004a, The Astrophysical Journal, 607, 1003
— 2004b, The Astrophysical Journal, 610, 1079
— 2005, The Astrophysical Journal, 624, 1010
- Brown, R. A., & Soummer, R. 2010, ApJ, 715, 122, doi: [10.1088/0004-637X/715/1/122](https://doi.org/10.1088/0004-637X/715/1/122)
- Bryson, S., Kunimoto, M., Kopparapu, R. K., et al. 2021, AJ, 161, 36, doi: [10.3847/1538-3881/abc418](https://doi.org/10.3847/1538-3881/abc418)
- Catanzarite, J., & Shao, M. 2011, PASP, 123, 171, doi: [10.1086/658243](https://doi.org/10.1086/658243)
- Chabrier, G. 2001, The Astrophysical Journal, 554, 1274, doi: [10.1086/321401](https://doi.org/10.1086/321401)
- Chauvin, G., Lagrange, A. M., Dumas, C., et al. 2004, A&A, 425, L29, doi: [10.1051/0004-6361:200400056](https://doi.org/10.1051/0004-6361:200400056)
- Crass, J., Gaudi, B. S., Leifer, S., et al. 2021, arXiv e-prints, arXiv:2107.14291. <https://arxiv.org/abs/2107.14291>
- Crepp, J. R., & Johnson, J. A. 2011, ApJ, 733, 126, doi: [10.1088/0004-637X/733/2/126](https://doi.org/10.1088/0004-637X/733/2/126)
- Davidson, J. M. 2011, PASP, 123, 923, doi: [10.1086/661725](https://doi.org/10.1086/661725)
- Dulz, S. D., Plavchan, P., Crepp, J. R., et al. 2020, ApJ, 893, 122, doi: [10.3847/1538-4357/ab7b73](https://doi.org/10.3847/1538-4357/ab7b73)
- Fang, J., & Margot, J.-L. 2012, ApJ, 761, 92, doi: [10.1088/0004-637X/761/2/92](https://doi.org/10.1088/0004-637X/761/2/92)
- Gaia Collaboration, Prusti, T., de Bruijne, J. H. J., et al. 2016, A&A, 595, A1, doi: [10.1051/0004-6361/201629272](https://doi.org/10.1051/0004-6361/201629272)
- Gaia Collaboration, Brown, A. G. A., Vallenari, A., et al. 2018, A&A, 616, A1, doi: [10.1051/0004-6361/201833051](https://doi.org/10.1051/0004-6361/201833051)
— 2021, A&A, 649, A1, doi: [10.1051/0004-6361/202039657](https://doi.org/10.1051/0004-6361/202039657)
- Gaskin, J. A., Swartz, D. A., Vikhlinin, A., et al. 2019, Journal of Astronomical Telescopes, Instruments, and Systems, 5, 021001, doi: [10.1117/1.JATIS.5.2.021001](https://doi.org/10.1117/1.JATIS.5.2.021001)
- Gaudi, B. S., Seager, S., Mennesson, B., et al. 2020, The Habitable Exoplanet Observatory (HabEx) Mission Concept Study Final Report. <https://arxiv.org/abs/2001.06683>
- Give'on, A., Kern, B., Shaklan, S., Moody, D. C., & Pueyo, L. 2007, in Astronomical Adaptive Optics Systems and Applications III, ed. R. K. Tyson & M. Lloyd-Hart, Vol. 6691, International Society for Optics and Photonics (SPIE), 63 – 73. <https://doi.org/10.1117/12.733122>
- Guimond, C. M., & Cowan, N. B. 2018, AJ, 155, 230, doi: [10.3847/1538-3881/aabb02](https://doi.org/10.3847/1538-3881/aabb02)
- Hill, M. L., Kane, S. R., Seperuelo Duarte, E., et al. 2018, ApJ, 860, 67, doi: [10.3847/1538-4357/aac384](https://doi.org/10.3847/1538-4357/aac384)
- Kane, S. R. 2013, ApJ, 766, 10, doi: [10.1088/0004-637X/766/1/10](https://doi.org/10.1088/0004-637X/766/1/10)
- Kane, S. R., & Blunt, S. 2019, AJ, 158, 209, doi: [10.3847/1538-3881/ab4c3e](https://doi.org/10.3847/1538-3881/ab4c3e)
- Kane, S. R., Mahadevan, S., von Braun, K., Laughlin, G., & Ciardi, D. R. 2009, PASP, 121, 1386, doi: [10.1086/648564](https://doi.org/10.1086/648564)
- Kane, S. R., Turnbull, M. C., Fulton, B. J., et al. 2020, AJ, 160, 81, doi: [10.3847/1538-3881/ab9ffe](https://doi.org/10.3847/1538-3881/ab9ffe)
- Kane, S. R., Hill, M. L., Kasting, J. F., et al. 2016, ApJ, 830, 1, doi: [10.3847/0004-637X/830/1/1](https://doi.org/10.3847/0004-637X/830/1/1)
- Kasting, J. F., Whitmire, D. P., & Reynolds, R. T. 1993, Icarus, 101, 108, doi: [10.1006/icar.1993.1010](https://doi.org/10.1006/icar.1993.1010)
- Kipping, D., Bryson, S., Burke, C., et al. 2022, Nature Astronomy, 6, 367, doi: [10.1038/s41550-021-01539-1](https://doi.org/10.1038/s41550-021-01539-1)
- Kopparapu, R. K., Ramirez, R. M., SchottelKotte, J., et al. 2014, ApJL, 787, L29, doi: [10.1088/2041-8205/787/2/L29](https://doi.org/10.1088/2041-8205/787/2/L29)
- Kopparapu, R. K., Ramirez, R., Kasting, J. F., et al. 2013, ApJ, 765, 131, doi: [10.1088/0004-637X/765/2/131](https://doi.org/10.1088/0004-637X/765/2/131)
- Kopparapu, R. K., Hébrard, E., Belikov, R., et al. 2018, ApJ, 856, 122, doi: [10.3847/1538-4357/aab205](https://doi.org/10.3847/1538-4357/aab205)
- Lissauer, J. J., Ragozzine, D., Fabrycky, D. C., et al. 2011, The Astrophysical Journal Supplement Series, 197, 8, doi: [10.1088/0067-0049/197/1/8](https://doi.org/10.1088/0067-0049/197/1/8)
- Lyon, R. G., & Clampin, M. 2012, Optical Engineering, 51, 011002, doi: [10.1117/1.OE.51.1.011002](https://doi.org/10.1117/1.OE.51.1.011002)
- Mamajek, E. 2019, Number Densities of Stars of Different Types in the Solar Vicinity, University of Rochester. http://www.pas.rochester.edu/~emamajek/memo_star_dens.html
- Mamajek, E. E., Prsa, A., Torres, G., et al. 2015, IAU 2015 Resolution B3 on Recommended Nominal Conversion Constants for Selected Solar and Planetary Properties, arXiv, doi: [10.48550/ARXIV.1510.07674](https://doi.org/10.48550/ARXIV.1510.07674).
<https://arxiv.org/abs/1510.07674>
- Marois, C., Macintosh, B., Barman, T., et al. 2008, Science, 322, 1348, doi: [10.1126/science.1166585](https://doi.org/10.1126/science.1166585)
- Mawet, D., Pueyo, L., Lawson, P., et al. 2012, Space Telescopes and Instrumentation 2012: Optical, Infrared, and Millimeter Wave, doi: [10.1117/12.927245](https://doi.org/10.1117/12.927245)
- Meixner, M., Cooray, A., Leisawitz, D., et al. 2019, arXiv e-prints, arXiv:1912.06213. <https://arxiv.org/abs/1912.06213>

- Morgan, R., Savransky, D., Stark, C., & Nielson, E. 2019, Standard Definitions and Evaluation Team Final Report, <https://exoplanets.nasa.gov/exep/studies/sdet/>
- Morgan, R., Savransky, D., Turmon, M., et al. 2021, *Journal of Astronomical Telescopes, Instruments, and Systems*, 7, 021220, doi: [10.1117/1.JATIS.7.2.021220](https://doi.org/10.1117/1.JATIS.7.2.021220)
- Peretz, E., Hall, N. K. D., Mather, J. C., Shaklenr, S. B., & Hildebrandt, S. R. 2021, *J. Astron. Telesc. Instrum. Syst.*, 7, doi: [10.1117/1.JATIS.7.2.029801](https://doi.org/10.1117/1.JATIS.7.2.029801)
- Plavchan, P., Bilinski, C., & Currie, T. 2014, *PASP*, 126, 34, doi: [10.1086/674819](https://doi.org/10.1086/674819)
- Savransky, D. 2013, in *Society of Photo-Optical Instrumentation Engineers (SPIE) Conference Series*, Vol. 8864, *Techniques and Instrumentation for Detection of Exoplanets VI*, ed. S. Shaklan, 886403
- Savransky, D., Kasdin, N. J. D., & Belson, B. A. 2009, in *Society of Photo-Optical Instrumentation Engineers (SPIE) Conference Series*, Vol. 7440, *Techniques and Instrumentation for Detection of Exoplanets IV*, ed. S. B. Shaklan, 74400B
- Shabram, M., Demory, B.-O., Cisewski, J., Ford, E. B., & Rogers, L. 2016, *The Astrophysical Journal*, 820, 93, doi: [10.3847/0004-637x/820/2/93](https://doi.org/10.3847/0004-637x/820/2/93)
- Shao, M., Catanzarite, J., & Pan, X. 2010, *ApJ*, 720, 357, doi: [10.1088/0004-637X/720/1/357](https://doi.org/10.1088/0004-637X/720/1/357)
- Stark, C. C., Roberge, A., Mandell, A., et al. 2015, *The Astrophysical Journal*, 808, 149, doi: [10.1088/0004-637x/808/2/149](https://doi.org/10.1088/0004-637x/808/2/149)
- Stark, C. C., Roberge, A., Mandell, A., & Robinson, T. D. 2014, *The Astrophysical Journal*, 795, 122, doi: [10.1088/0004-637x/795/2/122](https://doi.org/10.1088/0004-637x/795/2/122)
- Teachey, A., Kipping, D. M., & Schmitt, A. R. 2018, *AJ*, 155, 36, doi: [10.3847/1538-3881/aa93f2](https://doi.org/10.3847/1538-3881/aa93f2)
- Team, T. L. 2019, *The LUVVOIR Mission Concept Study Final Report*. <https://arxiv.org/abs/1912.06219>
- Traub, W. A., Breckinridge, J., Greene, T. P., et al. 2016, *Journal of Astronomical Telescopes, Instruments, and Systems*, 2, 011020, doi: [10.1117/1.JATIS.2.1.011020](https://doi.org/10.1117/1.JATIS.2.1.011020)
- van Belle, G. T., Meinel, A. B., & Meinel, M. P. 2004, in *Ground-based Telescopes*, ed. J. M. O. Jr., Vol. 5489, *International Society for Optics and Photonics (SPIE)*, 563 – 570. <https://doi.org/10.1117/12.552181>
- Zink, J. K., Christiansen, J. L., & Hansen, B. M. S. 2019, *MNRAS*, 483, 4479, doi: [10.1093/mnras/sty3463](https://doi.org/10.1093/mnras/sty3463)

APPENDIX

A. INDEX OF VARIABLE NAMES

Variable Name	Definition	Units
η_{\oplus}	The average number of earth-like planets hosted by a star.	Unitless
D_{lim}	The maximum distance away we will be looking.	Meters
N_*	The number of stars that we will observe.	Unitless
N_{\oplus}	The number of Exo-Earths that the survey aims to observe.	Unitless
ρ_*	The stellar density, assumed to be uniform.	cubic meter ⁻¹
ρ_{\oplus}	The density of Exo-Earths, also assumed to be uniform.	cubic meter ⁻¹
T	The total on-sky time.	Seconds
$R(\nu)$	The rate at which a star emits photons of a given frequency. All stars are assumed to be identical.	s ⁻¹
K	The ratio contrast ratio for the bandpass of interest.	Unitless
R_e	The rate at which the telescope observes photons on the Exo-Earth. Equivalent to $\frac{RKd^2\varepsilon}{16D_k^2}$	s ⁻¹
$\varepsilon(f)$	The laboratory efficiency, as a function of frequency.	Unitless
ν	The observational frequency.	Hertz
D_k	The distance to the k th star.	Meters
t_k	The amount of time spent on the k th star. $T = \sum_{k=0}^{N_*} t_k$	Seconds
d	The diameter of the telescope.	Meters
SNR	The signal-to-noise ratio of the observation. Equivalent to $\sqrt{N_e}$. Must be at least SNR_0 .	Unitless
SNR_0	The minimum acceptable signal-to-noise ratio.	Unitless
N_e	The number of photons detected by the telescope.	Unitless
c	The total cost of the survey.	\$
C	A scaling constant for the cost, such that $c = Cd^{2.5}$	\$/ (meters ^{2.5})
iwa	The inner working angle of the telescope. Approximated to be $iwa = \frac{n_i \lambda}{d}. \quad (32)$	Radians
u_k	The amount of usable time spent on the k th star.	Seconds
w_k	The amount of unusable time spent on the k th star	Seconds
t_f	The fraction of time usable for each star. Depends on a , s_c , and $\cos i$	Unitless
a	The semi-major axis of an Exo-Earth. Determined by the location of the star's habitable zone. For solar analogues, this is close to Earth's semi-major axis.	Meters
s_c	The projection of the inner-working-angle onto the sky. $D_k \cdot iwa$.	Meters
$\cos i$	The cosine of a planet's orbital inclination. Assumed to be uniform random.	Unitless

Variable Name	Definition	Units
t_a	The average fraction of time usable, for a random $\cos i$. Defined as $t_a = \int_0^1 t_f d \cos i.$	Unitless
λ	The observational wavelength. $\lambda = c/f$.	Meters
n	A group of variables, meant to simplify equations. Not η_{\oplus} -dependent. $n \equiv \frac{n_i \lambda}{a} \quad (35)$	Meters ⁻¹
m	Another group of variables. Not η_{\oplus} -dependent. $m \equiv \frac{16SNR_0^2}{RK\varepsilon} \left(\frac{3}{4\pi\rho_*} \right)^{2/3} \quad (36)$	Complicated
x_p	The x -position of an exoplanet, from the viewer's perspective, as a function of time. $x_p(t) = a \cos(t)$	Meters
y_p	The t position of an exoplanet, from the viewer's perspective, as a function of time. The y -axis is defined as the axis shortened by the exoplanet's inclination. $y_p(t) = a \sin(t) \cos i$	Meters